Cellular and Molecular Life Sciences (2018) 75:4557–4581
https://doi.org/10.1007/s00018-018-2911-z

Cellular and Molecular Life Sciences

ORIGINAL ARTICLE

miR-124-3p is a chronic regulator of gene expression after brain injury

Niina Vuokila[1] · Katarzyna Lukasiuk[2] · Anna Maria Bot[2] · Erwin A. van Vliet[3] · Eleonora Aronica[3,4] · Asla Pitkänen[1] · Noora Puhakka[1]

Received: 14 May 2018 / Revised: 2 August 2018 / Accepted: 22 August 2018 / Published online: 28 August 2018

Abstract

Traumatic brain injury (TBI) initiates molecular and cellular pathologies that underlie post-injury morbidities, including hippocampus-related memory decline and epileptogenesis. Non-coding small RNAs are master regulators of gene expression with the potential to affect multiple molecular pathways. To evaluate whether hippocampal gene expression networks are chronically regulated by microRNAs after TBI, we sampled the dentate gyrus of rats with severe TBI induced by lateral fluid-percussion injury 3 months earlier. Ingenuity pathway analysis revealed 30 upregulated miR-124-3p targets, suggesting that miR-124-3p is downregulated post-TBI (z-score = − 5.146, $p < 0.05$). Droplet digital polymerase chain reaction (ddPCR) and in situ hybridization confirmed the chronic downregulation of miR-124-3p ($p < 0.05$). Quantitative PCR analysis of two targets, *Plp2* and *Stat3*, indicated that their upregulation correlated with the miR-124-3p downregulation ($r = -0.647$, $p < 0.05$; $r = -0.629$, $p < 0.05$, respectively). Immunohistochemical staining of STAT3 confirmed the increased protein expression. STRING analysis showed that 9 of the 30 miR-124-3p targets belonged to a STAT3 network. Reactome analysis and data mining connected the targets especially to inflammation and signal transduction. L1000CDS2 software revealed drugs (e.g., importazole, trichostatin A, and IKK-16) that could reverse the observed molecular changes. The translational value of our data was emphasized by in situ hybridization showing chronic post-traumatic downregulation of miR-124-3p in the dentate gyrus of TBI patients. Analysis of another brain injury model, status epilepticus, highlighted the fact that chronic downregulation of miR-124 is a common phenomenon after brain injury. Together, our findings indicate that miR-124-3p is a chronic modulator of molecular networks relevant to post-injury hippocampal pathologies in experimental models and in humans.

Keywords Big data · Bioinformatics · microRNA · miR-124-3p · Traumatic brain injury

Introduction

Traumatic brain injury (TBI) affects approximately 10 million people worldwide each year [1]. In addition to the impact-induced primary injury, TBI triggers a cascade of secondary cellular pathologies, including progressive neuronal loss, axonal and myelin injury, and neuroinflammation. Many of these pathologies underlie the development of functional deficits in somatomotor and cognitive functions, as well as in mental health. On the other hand, some of them, like axonal plasticity and neurogenesis, can support the recovery process [2, 3]. The complexity of the post-TBI aftermath presents both a challenge and an opportunity for identifying molecular pathways that could be targeted by pharmacotherapies. One approach is to apply an unbiased genome-wide bioinformatics analysis to pinpoint the master regulators of molecular pathways that are modulated by TBI,

Electronic supplementary material The online version of this article (https://doi.org/10.1007/s00018-018-2911-z) contains supplementary material, which is available to authorized users.

✉ Asla Pitkänen
asla.pitkanen@uef.fi

✉ Noora Puhakka
noora.puhakka@uef.fi

[1] A.I. Virtanen Institute for Molecular Sciences, University of Eastern Finland, PO Box 1627, 70211 Kuopio, Finland

[2] The Nencki Institute of Experimental Biology, Polish Academy of Sciences, 3 Pasteur Str, 02-093 Warsaw, Poland

[3] Department of (Neuro)pathology, Academic Medical Center, University of Amsterdam, Meibergdreef 9, 1105 AZ Amsterdam, The Netherlands

[4] Stichting Epilepsie Instellingen Nederland (SEIN), Amsterdam, The Netherlands

and use them to design treatments to alleviate or prevent comorbidogenesis over the course of days to months after TBI.

MicroRNAs (miRNAs) are a class of small, 18–23 nucleotide long, non-coding RNAs [4]. miRNAs suppress gene expression by binding to the 3′ untranslated region of messenger RNA (mRNA) [4, 5], thereby preventing protein translation. As one miRNA can regulate hundreds of mRNAs, miRNAs control the expression of the entire protein network rather than an individual protein, allowing us to gain a more thorough understanding of disease pathology [6].

Previous studies in various experimental models of TBI demonstrated that TBI induces remarkable changes in miRNAs, in both the brain [7–20] and plasma/serum [21]. Studies in humans with various types of TBI also exhibit changes in miRNAs in the brain [22], plasma/serum [23–25], and cerebrospinal fluid [23, 26]. The first proof-of-concept studies demonstrated the potential of miRNA-based therapies to improve the post-TBI cellular outcome, particularly blood–brain barrier damage-related edema [27, 28], neuroinflammation, and neurogenesis [29], apoptosis [30, 31], and even post-TBI functional recovery [32]. Despite the evolution of functional impairments as well as recovery over a period of several months post-TBI [33–35], only one study has assessed the chronic regulation of transcriptomic changes [36].

Here we tested the hypothesis that bioinformatics analysis of chronic transcriptome data will reveal specific miRNAs regulating the expression of several proteins that form a molecular network related to ongoing chronic cellular pathologies after TBI. We chose to investigate the dentate gyrus that is one of the key brain areas involved in the post-TBI pathologies [37, 38], and the most damaged hippocampal subfield after lateral fluid-percussion injury [39].

Materials and methods

Animals

From an original cohort of 30 adult male Sprague–Dawley rats, 11 (body that weighed 300–354 g at the time of injury, Envigo, Horst, The Netherlands [36]) were used for the PCR analyses in the TBI experiment. The rest of the animals were used in another project. A separate cohort of 13 rats (350–400 g, Envigo, Udine, Italy) was used for in situ hybridization after TBI. In addition, 25 rats (350–400 g, Medical Research Centre, Warsaw, Poland) were used for PCR and in situ hybridization in SE experiments. Rats were housed in a controlled environment (temperature 22 ± 1 °C; humidity 50–60%; lights on from 07:00 to 19:00 h). Water and pellet food were provided ad libitum.

All animal procedures for TBI rats and SE rats were approved by the Animal Ethics Committee of the Provincial Government of Southern Finland and the Ethical Committee on Animal Research of the Nencki Institute, respectively. All animal work was carried out in accordance with the guidelines of the European Community Council Directives 2010/63/EU.

Human samples

Autopsy hippocampal samples were obtained from patients (Table 1) at the Department of Neuropathology at the Academic Medical Center (AMC) in Amsterdam, The Netherlands. Control samples ($n = 5$; 3 males, 2 females, median age 48, range 35–71) were obtained at the autopsy of adult subjects without any history of neurologic disease. All samples were collected within 24 h after death. Informed consent was obtained for the use of brain tissue and for access to the medical records. Tissue was obtained and used in accordance with the Declaration of Helsinki and the AMC Research Code provided by the Medical Ethics Committee.

Lateral FPI-induced TBI

Rats were subjected to lateral FPI (PCR, $n = 12$ controls, $n = 18$ TBI; in situ hybridization, $n = 3$ naïve, $n = 6$ control, $n = 6$ TBI) as described previously [40, 41]. Rats were anesthetized by intraperitoneal injection (6 ml/kg) of a mixture of sodium pentobarbital (58 mg/kg), magnesium sulfate (127.2 mg/kg), propylene glycol (42.8%), and absolute ethanol (11.6%), and placed in a Kopf stereotactic frame (David Kopf Instruments, Tujunga, CA, USA). The anesthetic cocktail used for the PCR cohort also contained 60 mg/kg chloral hydrate. A midline scalp incision was made and the underlying periosteum dissected. A 5-mm circular craniectomy was performed with a trephine over the left parietal lobe, midway between lambda and bregma, with the lateral edge of the craniectomy adjacent to the lateral ridge. A modified Luer–Lock cap was cemented into the craniectomy (Selectaplus CN, Dentsply DeTRey GmbH, Dreieich, Germany) and filled with saline. At 90 min after administration of the anesthesia, animals were connected to the fluid-percussion device (AmScien Instruments, Richmond, VA, USA) through the male Luer–Lock fitting and brain injury was induced (PCR: 3.20 ± 0.02 atm, in situ hybridization: 3.28 ± 0.13 atm; no difference between cohorts). Duration of apnea and occurrence of acute post-impact seizures were monitored. Sham-operated control animals received anesthesia and underwent all surgical procedures without lateral FPI. For PCR, we used the samples from animals (6 TBI and 5 controls) included in the original transcriptomic profiling [36].

Table 1 Patient information

Sex	Post-TBI	Age at time of death	Injury mechanism	Injury location	Injury severity GCS	Other diseases	Medication	Epilepsy (yes, no)	CT/MRI/brain	Other
f	1 m	57	Accident	Temporal L	Moderate	No	CBZ, LTG	Yes	CT: haemo.c contusions temp. L; tSAH	Bronchopneumonia
m	25 years	65	Accident	Frontal, temp. R/L	Mild	No	CBZ, LEV	Yes	NA	Myocardial infarction

Mild head injury (GCS score of 13–15), moderate head injury (GCS score of 9–12), traumatic subarachnoid hemorrhage (tSAH), traumatic subdural hematoma (tSDH), carbamazepine (CBZ), levetiracetam (LEV), lamotrigine (LTG)

Induction of SE with electrical amygdala stimulation

Induction of SE by electrical amygdala stimulation was performed as previously described in detail [42, 43]. Briefly, animals were anesthetized by an injection of butorphanol (Butomidor, Richter Pharma AG, Wells, Austria; 0.5 mg/kg ip). Surgery was performed under isoflurane anesthesia (2–2.5% in 100% O_2). A stimulating and recording bipolar wire electrode (Plastics One Inc., Roanoke, VA, USA #E363-3-2WT-SPC) was implanted into the left lateral nucleus of the amygdala 3.6 mm posterior and 5.0 mm lateral to bregma, 6.5 mm ventral to the brain surface [44]. A stainless steel screw electrode (Plastics One Inc. #E363/20) was implanted contralaterally into the skull over the right frontal cortex (3.0 mm anterior and 2.0 mm lateral to bregma) as a surface electroencephalography recording electrode. Two stainless steel screw electrodes were placed bilaterally over the cerebellum (10.0 mm posterior and 2.0 mm lateral to bregma) as ground and reference electrodes. The socket contacts of all the electrodes were placed in a multichannel electrode pedestal (Plastics One Inc. #MS363) that was attached to the skull with dental acrylate (Duracryl Plus). At 2 weeks post-operation, SE was induced by electrical stimulation via the intra-amygdala electrode. Stimulation comprised a 100-ms train of 1-ms biphasic square-wave pulses (400 µA peak to peak) delivered at 60 Hz every 0.5 s for 30 min. If the animal did not enter SE, stimulation was continued for an additional 10 min. The SE was intercepted after 1.5–2 h with an intraperitoneal injection of diazepam (20 mg/kg). If the first dose of diazepam did not suppress the SE, the animal received subsequent doses of diazepam at 5 mg/kg. Time-matched control animals had electrodes implanted but did not receive electrical stimulation.

Sampling of the dentate gyrus

Animals used for PCR after TBI and SE

The sampling and dentate gyrus dissection procedures were described in Puhakka et al. [36] for TBI animals and in Bot et al. [43] for SE animals. We used only the 7-days post-SE miRNA data published by Bot et al. [43] for comparative analysis, as these data well-correspond to the epileptogenesis phase [42, 45]. Briefly, rats were anesthetized with CO_2 at 7 day post-SE or 3 months post-TBI and decapitated with a guillotine. Their brains were removed, and the left hippocampus was dissected out and immersed in ice-cold RNAlater RNA Stabilization Reagent (#76106, Qiagen, Hilden, Germany). The hippocampus was then cut into thin coronal slices from which the dentate gyrus was separated (Fig. 1) and used for gene expression analysis. Samples were snap-frozen and stored at − 20 °C.

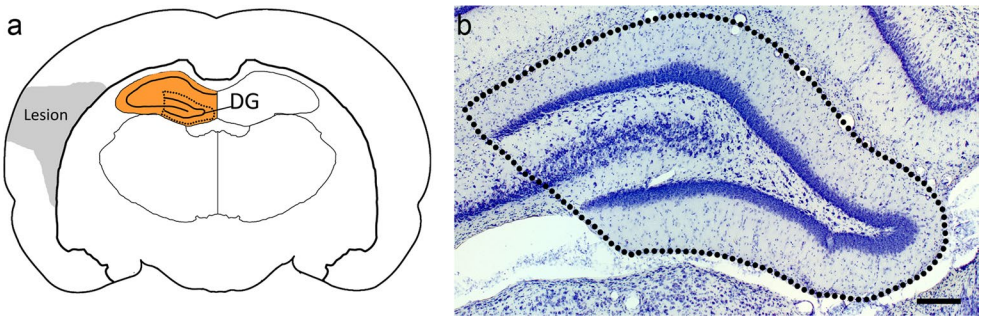

Fig. 1 Tissue sampling. At 3 months after traumatic brain injury (TBI), rats were decapitated. The ipsilateral dentate gyrus was dissected as shown with the dashed line in **a** the schematic drawing and **b** Nissl-stained section, and used for molecular analyses. Scale bar in **b** 200 µm

Animals used for in situ hybridization after TBI

To assess miR-124-3p cellular localization via in situ hybridization, the animals (3 naïve, 3 controls, 5 TBI) were perfused at 3 months post-TBI. Animals were anesthetized by an intraperitoneal injection of pentobarbital (60 mg/kg, ip). Thereafter, they were transcardially perfused with 0.9% sodium chloride solution (30–35 ml/min for 2 min) followed by 4% paraformaldehyde (PFA) in 0.1 M sodium phosphate buffer (PB), pH 7.4 (5 ml/min for 20 min). The brain was removed from the skull and post-fixed in 4% PFA in 0.1 M PB for 4 h.

After the post-fixation procedure, the brains were rinsed in tap water for 30 min and then placed in a Tissue-Tek Mega-Cassette (Sakura, #4173). They were infiltrated with paraffin as follows (Shandon Citadel 2000): 1 h in 50% ethanol; 1 h in 80% ethanol; 1 h, and then 2 h twice in 96% ethanol; 3 h, then 2 h twice in absolute ethanol; 30 min twice in xylene; and 2 h twice in paraffin. The paraffin-embedded brains were stored at room temperature.

The brains were cut into 6-µm-thick sections using a Microm 355 microtome with a Leica 818 blade and the sections were mounted on Superfrost microscope slides (Thermo Scientific, Gerhard Menzel GmbH, Braunschweig, Germany). One brain from the 3-month post-TBI group had to be removed from the analysis due to the poor quality of the sections.

Animals used for in situ hybridization after SE

At 7 day post-TBI, the rats were anesthetized with CO_2 and decapitated with a guillotine. The brains were quickly removed from the skull and fresh frozen in − 80 °C heptane. The samples were stored at − 80 °C until processed. The brains were cut into 10-µm-thick coronal sections using a cryostat. The sections were mounted on Superfrost® Plus slides (Thermo Scientific), dried at room temperature for 5 min, and stored at − 80 °C until use.

Human brain samples

Human brain tissue was fixed in 10% buffered formalin and embedded in paraffin. Paraffin-embedded tissue was sectioned at 5 µm, mounted on pre-coated glass slides (Star Frost, Waldemar Knittel, Braunschweig, Germany), and processed for in situ hybridization.

Bioinformatics analysis of upstream regulators of chronically altered gene expression after TBI

First, we analyzed gene expression in the rat dentate gyrus at 3 months after lateral FPI using the Affymetrix gene array [for details, see Puhakka et al. [36]. To determine the upstream regulators of gene expression with a focus on miRNAs, genes with significantly ($p < 0.05$) altered expression levels were included in the Ingenuity Upstream Regulator analysis using the Ingenuity Pathway Analysis (IPA) software (QIAGEN Redwood City, CA, USA, http://www.qiagen.com/ingenuity). The analysis revealed a significant change in 31 of 844 targets of the brain-enriched miR-124-3p, and we thus focused on further analyses of brain tissue on this miRNA. The protein–protein interactions between the 31 miR-124-3p target gene products were analyzed with STRINGv10 [46], and the results were visualized with Cytoscape [47].

To determine if the gene networks predicted by the STRING analysis were enriched in the gene expression data derived from the dentate gyrus, we performed Gene Set Enrichment Analysis (GSEA) [48, 49]. A pre-ranked gene list was created from the dentate gyrus gene expression data, containing 11,704 genes in the TBI dataset and 11,870 in the SE dataset. Genes on the pre-ranked list were divided into negative and positive groups based on the fold change in expression. The genes on the list were then ranked according to their p values: the greater the p value, the closer the rank to 0. A negative rank value indicated downregulation and a positive rank indicated upregulation of gene expression. The miR-124-3p targets and the genes derived from the STRING analysis were then pooled into a single gene

list (miR-124-3p interactome) and compared to the rank list. Based on the results of the STRING analysis and GSEA, two of the genes were selected for further quantitative reverse transcription PCR (qRT-PCR) analysis.

To further investigate the STRING protein networks, we used the gene set list (miR-124-3p interactome) to review their molecular function with Reactome v60 [50, 51, available at http://www.reactome.org]. In addition, we used L1000 Characteristic Direction Signature Search Engine (L1000CDS^2) that is based on the LINCS database (a library of integrated network-based cellular signatures) to compare miR-124-3p regulated gene network changes (miR-124-3p interactome) to the gene expression profile of human cell lines treated with various chemical compounds.

Reverse transcription

miRNA PCR

To validate the miRNA findings, total RNA was translated to complementary DNA (cDNA) with the TaqMan miRNA Reverse Transcriptase Kit (#4366596, Applied Biosystems, Foster City, CA, USA http://www.appliedbiosystems.com) according to the manufacturer's instructions. First, the total RNA concentration in the sample was assessed with a 2100 Bioanalyzer Instrument (Agilent Technologies, Santa Clara, CA, USA) using the manufacturer's RNA 6000 Nano Kit for mRNA samples and the Small RNA Analysis Kit for miRNA samples. The sample (15 µl) was prepared by mixing 7 µl of the RT master mix with 5 µl of RNA solution (10 ng RNA/5 µl nuclease-free water) and 3 µl of 5× RT primer for miR-124-3p (mmu-miR-124-3p). Reverse transcription was then performed using a T100™ Thermal Cycler (Bio-Rad Laboratories Inc, Hercules, CA, USA) as follows: 16 °C for 30 min, 42 °C for 30 min, 85 °C for 5 min, and 4 °C thereafter. Samples were stored at − 20 °C until further processing.

mRNA PCR

To validate the post-TBI change in the expression of miR-124-3p mRNA targets, 1 µg of total RNA from each sample was converted to cDNA using a High Capacity RNA-to-cDNA Kit (#4387406, Applied Biosystems) according to the manufacturer's protocol (http://tools.lifetechnologies.com/content/sfs/manuals/cms_047249.pdf).

Quantitative RT-PCR

Plp2 and *Stat3* mRNA

The PCR mixture was prepared using 12 ng of cDNA (RNA equivalents) as a template, gene-specific primers, and probes (pre-validated Taqman Gene Expression Assay for *Plp2* ID: Rn01525076_g1; *Stat3* ID: Rn01456553_m1, and *Gapdh* (internal control) ID: Rn99999916_s1, Applied Biosystems), and TaqMan Gene Expression Master Mix (Applied Biosystems). Quantitative RT-PCR was run with the StepOnePlus Real-Time PCR System (Applied Biosystems) as follows: 95 °C for 10 min, then 40 cycles (15 s each) at 95 °C and 60 °C for 60 s. A five-point standard curve was prepared using 75 ng, 37.5 ng, 18.8 ng, 9.4 ng, and 4.7 ng of cDNA as the template. Quantity values were normalized relative to *Gadph* according to the following formula: $\text{Quantity}_{\text{Norm}} = \text{Quantity(gene of interest)}/C_t(Gapdh)$.

miR-124-3p

The miR-124 expression in the brain samples at 7 day post-SE was determined from the same miRNA samples used for the microarray experiment [43]. Reverse transcription was performed using TaqMan® microRNA Reverse Transcription kit (#4366596, Thermo Fisher Scientific) according to the manufacturer's instruction. Real-time PCR was performed in triplicate with the cDNA template in a 20-µl reaction volume. The reaction contained 2× TaqMan Universal Master Mix, no UNG (#4440047, Thermo Fisher Scientific), and probe for miR-124-3p (Thermo Fisher Scientific). Quantitative PCR was run using the 7900HT Fast Real-Time System (Applied Biosystems) under the following conditions: 95 °C for 10 min, then 40 cycles of 95 °C for 15 s, followed by 60 °C for 60 s. The miRNA expression was normalized to miR-9a-5p. Fold changes were calculated by the $2^{-\Delta\Delta Ct}$ method (Livak and Schmittgen 2001).

Droplet digital PCR

The amount of mature miR-124-3p in the dentate gyrus at 3 months post-TBI was determined with ddPCR. Reaction mixtures were prepared as described in Bio-Rad's Droplet Digital™ PCR Applications Guide (Bio-Rad, http://www.bio-rad.com/). Briefly, for each 20 µl reaction, 1.33 µl of cDNA was mixed with 1 µl of TaqMan Small RNA Assay (20×), 10 µl of Bio-Rad's ddPCR supermix for probes, and 7.67 µl nuclease-free water (#AM9939, Ambion, Austin, TX, USA). Samples were loaded into the middle row of DG8 Cartridges (#1864008, Bio-Rad). Then, 70 µl of Droplet Generation Oil for Probes (#1863005, Bio-Rad) was added to the bottom wells of the cartridge. The cartridge was covered with a DG8™ Gasket (#1863009 Bio-Rad) and placed into the QX200 droplet generator (Bio-Rad). After droplet generation was completed, droplets (40 µl) were gently pipetted into the wells of a 96-well PCR plate (#951020303, Eppendorf, Hamburg, Germany), and the plate was sealed with pierceable sealing foil (#1814040 Bio-Rad) using a PX1 PCR Plate Sealer (Bio-Rad). PCR was run using the PTC-200 Thermal Cycler (ramp rate 2 °C/s; MJ Research)

under the following conditions: 95 °C for 10 min, then 40 cycles (15 s each) at 95 °C followed by 1 cycle at 60 °C (60 s), and finally, 98 °C for 10 min (see Miotto et al. [52]). After the PCR, the fluorescence of each droplet was measured with a QX100 Droplet Reader (Bio-Rad). The results were analyzed with QuantaSoft software v1.7 (Bio-Rad) to determine the copy number of miR-124-3p in each sample. All samples were run as triplets. The amounts of positive droplets in the triplets were combined together and used for statistical analysis.

In situ hybridization

TBI model

Sections were deparaffinized with xylene three times for 3 min each, followed by 1 min twice in absolute ethanol and 1 min in 70% ethanol and finally, washed with water. To undo protein crosslinking, the sections were incubated in a 90 °C water bath in preheated citrate buffer (0.1 M citric acid and 0.1 M trisodium citrate mixed 11.5:88.5, pH 6.0) for 90 min and then washed with Milli-Q water. In situ hybridization for miR-124-3p was performed using 5′–3′ fluorescein (FAM)-labeled probes (FAM-GgcAuuCacCgcGugCcuuA [capital letters indicate locked nucleic acids, whereas lower case letters indicate 2′-*O*-methylated nucleic acids], RiboTask APS, Odense, Denmark). Sections were prehybridized in hybridization mix (50% vol/vol formamide, 600 mM NaCl, 10 mM HEPES buffer pH 7.5, 5× Denhardt's reagent, 200 µg/ml denatured herring sperm DNA [D6898, Sigma-Aldrich, St. Louis, MO, USA]) for 15 min at 56 °C in a hybridization oven. The probe was diluted with hybridization mix to a final concentration of 500 nM and heated for 5 min at 95 °C while shaking before hybridization. Sections were hybridized for 1 h at 56 °C in the hybridization oven. After hybridization, the sections were washed with 2× saline–sodium citrate buffer (SSC; #A1396,1000, AppliChem, Darmstadt, Germany) buffer for 2 min, 0.5× SSC for 2 min at hybridization temperature, and then in 0.2× SSC for 1 min while shaking, and finally twice with PBS at room temperature. The sections were blocked with blocking buffer (1% bovine serum albumin, 0.02% Tween20, 1:100 normal goat serum) for 15 min. The signal was detected by incubating the sections with alkaline phosphate-labeled anti-fluorescein (Roche Diagnostics, Mannheim, Germany) diluted 1:500 in blocking buffer for 1 h. Section were washed three times with PBS and twice in TBS-Tween (0.05 M Tris, 0.15 M NaCl, 0.1% Tween20). Color was developed in NBT/BCIP (nitro-blue tetrazolium chloride)/5-bromo-4-chloro-3′-indolylphosphate *p*-toluidine salt, Roche Diagnostics, Mannheim, Germany) diluted 1:50 to NTM-T buffer (100 mM Tris, pH 9.5, 100 mM NaCl, 50 mM $MgCl_2$, 0.05% Tween20) for 40 min. Sections were washed with Milli-Q water, air-dried for 10 min, and coverslipped.

SE model

In situ hybridization was performed using LNA probes complementary to miR-124-3p and labeled with digoxigenin at both the 3′ and 5′ ends (EQ-88066-15, Exiqon). Hybridizations with LNA scramble-miR probe (EQ-99004-15, Exiqon) were used as a negative control. Briefly, the cryosections were thawed, fixed in 4% PFA, followed by gentle stirring in 0.1 M ethanolamine and 2.5% acetic anhydride for 10 min to block the endogenous alkaline phosphatase activity. Prehybridization was performed for 2 h in the hybridization oven with 500 ml of prehybridization buffer: 50% formamide, 5× SSC, 5× Denhardt's, 500 mg/ml salmon sperm DNA, and 2% blocking reagent (Roche) in diethyl pyrocarbonate-treated water. The probes were hybridized in 50% formamide, 5× SSC, 5× Denhardt's solution, 500 µg/ml salmon sperm DNA, and 2% blocking reagent diethyl pyrocarbonate-treated water overnight at 60 °C. After post-hybridization washes with 50% formamide, 2× SSC at 60 °C, and 2× SSC at room temperature, sections were blocked and incubated overnight with mouse anti-digoxigenin-AP (1:500, Roche), and the signal was visualized using BCIP/NBT (Roche). When each probe yielded a strong signal, the reactions were stopped by washing with PBS. The signal was visualized by standard light microscopy.

Human samples

In situ hybridization was carried out with the same protocol used for TBI rat samples, but with a probe concentration of 250 nM.

STAT3 immunohistochemistry

For STAT3 immunohistochemistry we used 25-µm-thick sections from our tissue bank. Sections were obtained from 6 TBI animals (3 months post-TBI) and 3 control animals (1 from 3 months post-operation, 2 from 1 month post-operation). For each animal, we stained two sections (sections 300 µm apart from each other).

First, the sections were washed three times with 0.02 M KPBS pH 7.4. To remove the endogenous peroxidase activity, the sections were incubated in 1% H_2O_2 in 0.02 M KPBS at room temperature for 15 min. The sections were washed three times with 0.02 M KPBS. Thereafter, sections were incubated in preheated 0.05 M sodium citrate buffer (pH 6.0) at 80 °C for 30 min and washed three times with 0.02 M KPBS. Non-specific binding was blocked with blocking buffer [10% normal horse serum (NHS) and 0.5% Triton-X in KPBS] for 2 h at room temperature. Sections

were incubated for 2 days at + 4 °C in the mouse monoclonal anti-STAT3 antibody (#ab119352, Abcam, Cambridge, UK) diluted 1:2000 with a solution containing 1% NHS and 0.5% Triton-X in KPBS. The sections were washed three times (2% NHS in 0.02 M KPBS) and incubated for 1 h with biotinylated anti-mouse secondary antibody (1:200, #BA-2000, Vector Laboratories, Burlingame, CA, USA) at room temperature. Thereafter, the sections were washed three times with KPBS, incubated for 45 min in avidin–biotin solution (1:200, PK-4000, Vector Laboratories), and washed three times with KPBS. Steps from the secondary antibody to the KPBS wash were repeated with recycled antibody and avidin–biotin solution. The secondary antibody was visualized with 0.1% 3,3′-diaminobenzidine (Pierce Chemicals, Rockford, IL, USA) and 0.08% H_2O_2 in 0.02 M KPBS (1 min at room temperature). The sections were then washed with KPBS and 0.1 M PB. Thereafter, sections were dried overnight at 37 °C. The color was intensified with osmium (OsO_4) thiocarbohydrate according to the method of Lewis et al. [53].

Parvalbumin immunohistochemistry

To investigate if miR-124 is regulated in inhibitory interneurons, we chose to conduct parvalbumin immunohistochemistry as this subclass of interneurons is the most vulnerable to lateral FPI [36]. For parvalbumin immunohistochemistry we used 6-µm-thick sections of paraffin-embedded brain. We conducted in situ hybridization as described previously, with exception that after deparaffinization the endogenous peroxidase was blocked with 0.3% H_2O_2 in methanol. After developing the color with NBT/BCIP, sections were washed three times with 0.02 M KPBS. To prevent non-specific binding, sections were incubated 2 h in the blocking buffer [10% normal horse serum (NHS) and 0.5% Triton-X in KPBS]. Next, sections were incubated 3 nights at + 4 °C in mouse monoclonal antibody raised against PARV (Swant, Bellizona, Switzerland) diluted 1:1000 in solution containing 1% NHS and 0.5% Triton-X in KPBS. Sections were washed three times in 2% NHS diluted to 0.02 M KPBS and incubated for 2 h with biotinylated anti-mouse secondary antibody (1:100, # BA-2000, Vector Laboratories, Burlingame, CA, USA) at room temperature. Next, sections were washed with 2% NHS in KPBS and incubated for 2 h in avidin–biotin solution (1:100, PK-4000, Vector Laboratories). Thereafter, sections were washed with 2% NHS in KBPS and the secondary antibody was vizualised with 0.1% 3,3′-diaminobenzidine (Pierce Chemicals, Rockford, IL, USA) and 0.08% H_2O_2 in 0.02 M KPBS (5 min at room temperature). The sections were then washed with KPBS and 0.1 M PB. Thereafter, sections were dried overnight at 37 °C and coverslipped.

Assessment of the intensity of miR-124-3p in situ hybridization and STAT3 immunohistochemistry

The RGB digital photographs of miR-124-3p in situ hybridization and STAT3 immunolabeling were obtained with an Axio Imager M2 microscope (Carl Zeiss Microimaging GmbH). All images were captured with identical exposure parameters using a 20× objective. ZEN 2 software (Carl Zeiss Microimaging GmbH) was used for image processing. The staining intensity was measured from digital photographs using ImageJ software by drawing a region of interest (ROI) around the dentate gyrus (see Fig. 1) at AP level − 2.8 from bregma. The color threshold was adjusted to be comparable to the staining intensity of the original RGB photomicrograph. The RGB images were then converted to grayscale. The mean optical density was measured from the whole dentate gyrus ROI. Background staining (background ROI) was measured from the fimbria for in situ hybridization analysis and from the internal capsule for immunohistochemistry analysis. Staining density was calculated by the following equation: (mean intensity of background ROI − mean intensity of the ROI)/mean intensity of background ROI. For technical restrictions, the in situ hybridization analysis was performed with one section per animal, whereas the STAT3 staining analysis was conducted on two sections per animal, and statistical tests were performed using the mean intensity of the two sections.

To further confirm that the miR-124 downregulation was not caused by neuronal loss, we measured the mean intensity of 100 cells inside the ROI (50 cells located in the CA3c area and 50 cells in the granule cell layer). The density was assessed using same equation and background ROI described above.

The changes in miR-124 expression in human samples were analyzed by measuring the intensity of in situ hybridization from a total of 150 cells per patient along the granule cell layer as well as 30–50 cells in the CA3. The mean intensity of the TBI cases was compared with that of all controls combined. The change in the miR-124 level is presented as a percentage compared with the control level.

Assessment of post-TBI neuronal loss

To determine the possible contribution of neuronal loss to the downregulation of miRNAs, we assessed the severity of neurodegeneration in Nissl-stained preparations (for the detailed protocol, please see Huusko et al. [39]) from the dentate gyrus at 3 months post-TBI. We then analyzed the expression of miR-124-2 and miR-124-3, the two preforms of mature miR-124, which would be expected to

decrease if expression of the mature form was due solely to neurodegeneration.

To investigate the localization of miR-124 after TBI, we performed in situ hybridization on a small subset of 7 day post-TBI sections from our tissue bank. In situ hybridization was conducted as described above. To examine the subcellular localization of miR-124, we counterstained some of the sections with hematoxylin and eosin (H&E; #03971 and #HT110116, Sigma-Aldrich). To investigate the cell-type specific localization of miR-124, we double-labeled the sections with NeuN (neuronal nuclei, MAB377, clone A60, Chemicon, Temecula, CA, USA), Iba1 (microglia, 019-19741, WAKO, Tokyo, Japan), and glial fibrillary acidic protein (GFAP; astrocytes, G-3893, Clone G-A-5, Sigma-Aldrich, Munich, Germany) using a BrightVision plus kit (Immunologic, Duiven, The Netherlands) and 3,3-diaminobenzidine (AEC) as the chromogen. After in situ hybridization, the sections were washed three times with PBS and incubated with primary antibody (NeuN 1:2000, Iba1 1:200, GFAP 1:2000) for 60 min at room temperature. The sections for the anti-NeuN immunohistochemistry were then washed three times with PBS and then blocked with post-antibody blocking solution (included in the BrightVision plus kit) for 15 min at room temperature. All sections were then washed three times with PBS. Next poly-HRP-GAMs/Rb IgG solution was pipetted onto the sections and the slides were incubated for 30 min at room temperature. Peroxidase activity was detected with AEC (in 0.05 M saline buffer, pH 4.9 with 0.01% H_2O_2). Thereafter, the sections were incubated with AEC for 8 min in the dark. The reaction was stopped by washing the sections first with deionized water and then with tap water. The sections were dehydrated by incubating them for 1 min in 70% ethanol, then twice for 1 min in absolute alcohol, and three times in xylene. Sections were coverslipped with glycerol gelatin.

Comparison of miR-124-3p expression after TBI to that after SE

We obtained previously published [43] miRCURY LNA™ microRNA Array 7th (#208500, Exiqon, Denmark) and GeneChip® Rat Gene 1.1 ST array (Affymetrix, Santa Clara, CA, #901627) data from 7 day post-SE rats. The microRNA array was used to investigate the miR-124 expression. The transcriptomics data was used to generate the rank list for GSEA analysis, as described above. To compare the TBI and SE models, enrichment of the 31 targets of miR-124 as well as the STRING network were compared to the SE rank list.

Data analysis

Statistical analyses were performed using IBM SPSS Statistics 21.0 (IBM Corp., Armonk, NY, USA). Differences in the qRT-PCR, ddPCR, and density analysis between control and TBI and SE animals were analyzed using the Mann–Whitney *U* test. Correlations between the miR-124-3p copy number in ddPCR and the intensity of the expression of each of its 31 target mRNAs in the array were determined with Spearman's test. Similarly, correlation of the miR-124-3p copy number with the relative quantity of *Plp2* and *Stat3* in qRT-PCR was determined with Spearman's test. To detect possible outliers, we performed the Grubbs' test using GraphPad's online calculator (available: https://www.graphpad.com/quickcalcs/grubbs2/). One control animal among the seven post-SE animals was identified as an outlier ($p < 0.05$) based on the qRT-PCR results. Thus, the animal was excluded from the further analysis of the qRT-PCR results. A p value less than 0.05 was considered statistically significant. All data are presented as mean ± SEM.

The function of the miR-124 targets was also assessed with text mining. The Scopus database was used to compile keywords from articles related to the targets. For each target, the search terms "gene name, e.g., *Stat3*" and "gene" were used. From the search results, 2000 latest articles (before December 20th, 2017) for each miR-124 target were included into the analysis. Word Cloud Generator (https://www.jasondavies.com/wordcloud/) was used to visualize the most common key words. In the visualization, the spiral "Archimedean" and the scale "logarithm of n" were used.

Results

Mortality

TBI PCR

Acute mortality within 48 h post-TBI was 22% (4/18). One rat died due to an unknown cause during the follow-up.

TBI in situ hybridization

Acute mortality within 48 h post-TBI was 17% (1/6). One control rat died during the surgery.

Bioinformatics analysis predicted the miR-124-3p downregulation at 3 months post-TBI

IPA analysis for upstream regulators revealed 31 genes (Bmp6, C2orf88, Ccl2, Cdk6, Ctdsp1, Eci2, Foxq1, Frmd8, Gsn, Lamc1, Limch1, Lrrc57, Myo10, Plp2, Ppfibp2, Prkd1, Prrx1, Ptbp1, Rab27a, Rbms1, Rhoj, Slc7a2, Stat3, Swap70, Tjp2, Tln1, Tmbim1, Tom1L1, Vat1, Vim, Zfp36l2) with a common predicted regulator, miR-124-3p ($p < 0.05$). Of these, 30 genes were upregulated and 1 (*Lrrc57*) was downregulated. The activation z-score for miR-124-3p was

Table 2 Targets of miR-124-3p according to ingenuity pathway analysis and their expression in the dentate gyrus at 3 months post-TBI

Gene symbol	Gene description	Fold change
Bmp6	Bone morphogenetic protein 6	1.24**
C2orf88	Chromosome 2 open reading frame 88	1.44**
Ccl2	Chemokine (C–C motif) ligand 2	1.10**
Cdk6	Cyclin-dependent kinase 6	1.16*
Ctdsp1	CTD (carboxy-terminal domain, RNA polymerase II, polypeptide A) small phosphatase 1	1.16*
Eci2	Enoyl-CoA delta isomerase 2	1.14**
Foxq1	Forkhead box Q1	1.11*
Frmd8	FERM domain containing 8	1.08*
Gsn	Gelsolin	1.36***
Lamc1	Laminin, gamma 1	1.12*
Limch1	LIM and calponin homology domains 1	1.10*
Lrrc57	Leucine rich repeat containing 57	− 1.14*
Myo10	Myosin X	1.13*
Plp2	Proteolipid protein 2 (colonic epithelium-enriched)	1.28***
Ppfibp2	PTPRF interacting protein, binding protein 2 (liprin beta 2)	1.11*
Prkd1	Protein kinase D1	1.12**
Prrx1	Paired related homeobox 1	1.11**
Ptbp1	Polypyrimidine tract binding protein 1	1.13*
Rab27a	RAB27A, member RAS oncogene family	1.17*
Rbms1	RNA binding motif, single stranded interacting protein 1	1.13*
Rhoj	ras homolog gene family, member J	1.09*
Slc7a2	Solute carrier family 7 (cationic amino acid transporter, y + system), member 2	1.20**
Stat3	Signal transducer and activator of transcription 3	1.12**
Swap70	SWAP switching B-cell complex 70	1.09*
Tjp2	Tight junction protein 2	1.13*
Tln1	Talin 1	1.13*
Tmbim1	Transmembrane BAX inhibitor motif containing 1	1.14**
Tom1L1	Target of myb1 like 1 membrane trafficking protein	1.08*
Vat1	Vesicle amine transport protein 1 homolog (T californica)	1.17*
Vim	Vimentin	1.53**
Zfp36l2	Zinc finger protein 36, C3H type-like 2	1.15*

*$p < 0.05$, **$p < 0.01$, ***$p < 0.001$

− 5.146, which suggested its downregulation. The gene expression changes are summarized in Table 2.

STRINGv10 was used to explore the protein–protein interactions between the protein products of the above given 31 target genes. Nine of them (CCL2, CDK6, GSN, PRLD1, RBMS1, STAT3, TJP2, TLN1, TOM1L1) formed a network (Fig. 2a). When other targets were reanalyzed individually, 16 other networks were discovered (Fig. 2a).

To validate the IPA analysis, we compared the miR-124-3p target gene list to the Affymetrix array data with GSEA. As expected, the upregulated targets were positively enriched with an enrichment score (ES) of 0.92 and false discovery rate (FDR) of less than 0.01 (Fig. 2b1). In addition, to determine if some of the networks were enriched in the gene expression analysis of the dentate gyrus, all genes encoding proteins belonging to the STRING networks were pooled. The GSEA of the 144 genes revealed that 86 (59%) were present in the ranking list (data not shown). Of these 86 genes, 30 were enriched with a score of 0.53 and an FDR of < 0.01 (Fig. 2b2), and thus upregulated in the expression data (black circles in Fig. 2a). Among these 30 genes, 24 were miR-124-3p targets. Of the miR-124-3p targets, Plp2 was the most enriched and thus chosen for qRT-PCR validation. The ranks of the proteins varied between 9 and 633. The Reactome analysis (Table 3) and data mining (Fig. 2c) connected the miR-124 targets and interactome especially to signal transduction, the immune system, gene expression, and proliferation. The top 20 most regulated molecular pathways in the Reactome analysis are presented in Table 3.

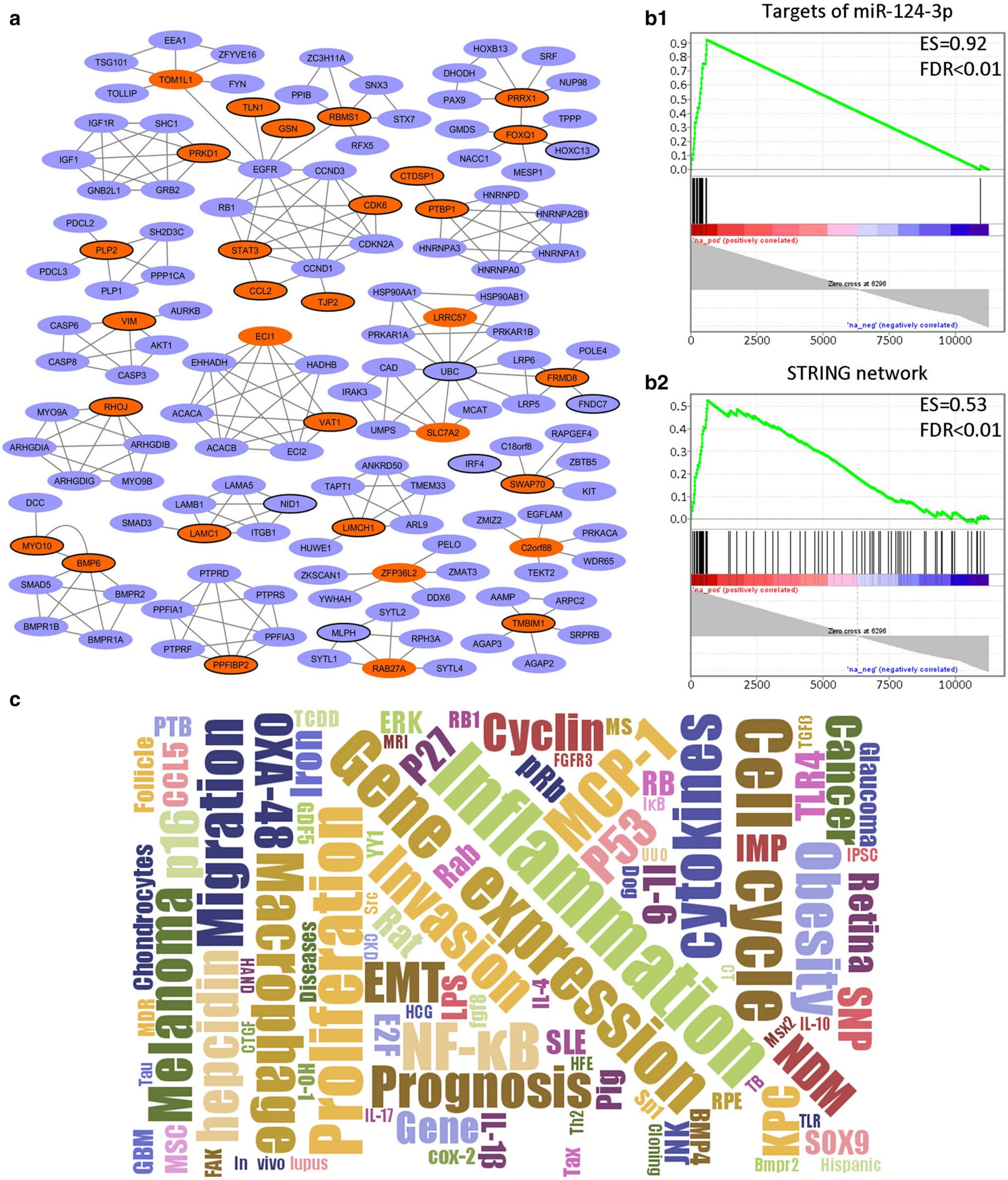

PCR validation confirmed the downregulation of miR-124-3p and upregulation of its targets after TBI

To confirm the bioinformatics-based prediction of miR-124-3p downregulation at 3 months post-TBI, we performed ddPCR analysis of miR-124-3p in the same samples from the dentate gyrus that were used for the gene expression analysis. Our data revealed significant downregulation of miR-124-3p expression (FC = 0.88, $p < 0.05$) compared

◂**Fig. 2** Enrichment of genes coding protein networks targeted by miR-124-3p at 3 months after TBI. **a** STRING analysis of miR-124 targets revealed 17 networks. From 31 targets, 9 (CCL2, CDK6, GSN, PRLD1, RBMS1, STAT3, TJP2, TLN1, TOM1L1) belonged to a "STAT3 network". According to GSEA, 24 of 31 miR-124-3p targets were enriched in the dataset (**b1**, ES = 0.92, FDR < 0.01). The genes coding the proteins in the STRING network (**a**) were pooled and analyzed with Gene Set Enrichment Analysis (GSEA) (**b2**). From them, 30 of 86 were enriched in the original dataset (ES = 0.53, FDR < 0.01). Color codes: orange, miR-124-3p target; black circle around orange, enriched in the GSEA; black circle around blue, enriched in the GSEA; blue, proteins added to the network by the STRING analysis. The most enriched gene was *Plp2*. **c** Text mining highlights the role of miR-124 targets in inflammation and proliferation. The word cloud presents the most common keywords among articles related to the 30 upregulated miR-124 targets after TBI. *ES* enrichment score, *FDR* false discovery rate. Annotations for proteins are presented in Online Resource 1

with controls (Fig. 3a). Moreover, receiver operating curve analysis indicated that at 3 months post-TBI, the reduced miR-124-3p expression in the dentate gyrus differentiated TBI animals from controls (area under the curve 0.883, $p < 0.05$).

Stat3 was selected for wet lab analysis as it is a direct target of miR-124-3p [55], and is activated after TBI [56, 57] and pilocarpine-induced SE [58]. To also analyze genes outside the STAT3 network, Plp2 was selected for validation as the most enriched gene in GSEA. Subsequent qRT-PCR showed a 1.7-fold upregulation of *Plp2* and a 1.4-fold upregulation of *Stat3* ($p < 0.01$, Fig. 3b, c).

We then correlated the miR-124-3p expression level in ddPCR with the expression levels of its 31 target genes in the array (Fig. 3d). Expression of 33% (6 of 18) of the target genes negatively correlated with the expression of miR-124-3p ($p < 0.05$). Notably, miR-124-3p expression was negatively correlated with *Plp2* expression in the array ($r = -0.770$, $p < 0.01$), whereas it only tended to negatively correlate with *Stat3* expression ($p = 0.053$). On the other hand, miR-124-3p expression was significantly negatively correlated with the qRT-PCR results of both *Plp2* ($r = -0.647$, $p < 0.05$; Fig. 3e) and *Stat3* ($r = -0.629$, $p < 0.05$; Fig. 3f).

In situ hybridization confirmed miR-124 downregulation and addresses differential expression of miR-124 in subfields of dentate gyrus

In situ hybridization of miR-124-3p was conducted to investigate the site of the downregulated miR-124-3p in more detail at 3 months post-TBI (Fig. 4b) compared with control animals (Fig. 4a). At 3 months post-TBI, miR-124 was 27-fold downregulated compared with controls (Fig. 4c, $p < 0.01$). To further pinpoint the layer-specific downregulation of miR-124, we measured the staining intensity in 50 cells in each section of the CA3c and granule cell layer. The analysis revealed no difference between the control and TBI groups in the CA3c, but a robust downregulation of miR-124 after TBI in the granule cell layer (Fig. 4d, FC = 0.62, $p < 0.01$).

Next, we quantified the immunohistochemical staining intensity of one of the miR-124-3p targets, STAT3. Our analysis showed a fourfold upregulation of STAT3 ($p < 0.05$, Fig. 5) at 3 months post-TBI.

We subsequently extended the miR-124-3p in situ hybridization analysis to the human dentate gyrus samples. We compared the intensity of the in situ hybridization between patients with no known neurologic disease and patients with TBI. Our analysis revealed that miR-124 robustly decreased post-TBI in both the granule cell layer (91% at 1 month and 39% at 25 years compared with controls) and CA3 area (91% at 1 month and 69% at 25 years compared with controls; Fig. 6).

Does neuronal loss explain the reduction in miR-124-3p after TBI?

Lateral FPI results in ~ 50% loss of hilar neurons and 10% loss of granule cells in the dentate gyrus [39, 41, 54]; (Fig. 7a–c). Therefore, we wondered whether the observed miR-124-3p downregulation could be explained simply by neurodegeneration. Our array data in the dentate gyrus, however, indicated that expression of the long premature forms of miR-124-3p, i.e., miR-124-2 and miR-124-3, was comparable to that in controls (Fig. 7d, e). If neurodegeneration accounted for the downregulation, then the levels of miR-124-3p premature forms would also be decreased. Thus, these data suggest that the reduction in miR-124-3p is related to impaired miRNA processing.

To determine where in the cell and in which brain cell type miR-124 is expressed, we prepared sections with miR-124 in situ hybridization (Fig. 7f) combined with either hematoxylin and eosin staining (Fig. 7g) or immunohistochemical staining of microglial, astrocytic, and neuronal markers (Fig. 7h–m). Together these histologic preparations confirmed that in control rats and after TBI, miR-124 is expressed in the cytosol and solely in neurons. Moreover, we showed that in addition to excitatory granule cells (Fig. 7j–m), miR-124 is downregulated also in the parvalbumin-positive interneurons (Fig. 7n–q).

miR-124-3p expression at 7 days after SE is similar to chronic TBI

Finally, we compared the miR-124-3p expression after lateral FPI to the SE model. We focused our analysis on 7 day post-SE samples, representing the epileptogenesis phase. The miRCURY microRNA array indicated downregulation of miR-124-3p at 7 days post-SE ($p < 0.01$, Fig. 8a).

Table 3 The reactome analysis of proteins in the STRING network connects the targets of miR-124 to several immune system-related pathways

Pathway name*	Entities found**	Entities *p* value
Signal transduction	65	4.32E−05
Immune system	57	2.77E−04
Cytokine signaling in immune system	38	2.05E−08
Innate immune system	37	7.87E−04
Signaling by interleukins	35	4.02E−11
Developmental biology	32	1.92E−04
Axon guidance	27	1.19E−07
Signaling by NGF	25	1.02E−07
Downstream signal transduction	23	8.43E−09
DAP12 signaling	23	9.70E−09
DAP12 interactions	23	2.10E−08
Signaling by PDGF	23	3.39E−08
NGF signaling via TRKA from the plasma membrane	23	4.55E−08
Signaling by EGFR	22	6.96E−08
VEGFA–VEGFR2 pathway	20	3.76E−07
Signaling by VEGF	20	5.44E−07
IGF1R signaling cascade	19	2.25E−07
Signaling by type 1 insulin-like growth factor 1 receptor (IGF1R)	19	2.36E−07
Signaling by SCF-KIT	19	1.30E−06
Cell cycle	19	3.32E−03

*Twenty pathways with most mapped proteins are presented. **"Entities found" refers to the number of mapped proteins that match the pathway

Quantitative RT-PCR validated the downregulation in the same samples (FC = 0.82, $p < 0.05$, Fig. 8b). Similar to TBI analysis, transcriptomic profiling data after SE showed an upregulation of two miR-124-3p targets, *Plp2* ($p < 0.01$, Fig. 8c) and *Stat3* ($p < 0.01$, Fig. 8d). Next, we used GSEA to compare the expression of the 31 differentially expressed targets in the TBI dataset. Of these, 15 were positively enriched at 7 days post-SE (ES = 0.657, FDR < 0.01, Fig. 8e). Among the 144 genes belonging to the miR-124 interactome, 22 were positively enriched in the SE dataset (ES = 0.322, FDR < 0.05, Fig. 8f). Importantly, qualitative analysis of in situ hybridization of miR-124-3p showed a detectable downregulation of miR-124-3p (Fig. 8g, h) after SE as compared to a control rat.

L1000CDS predicted novel compounds to reverse the miR-124-3p-dependent signature after TBI

We used the L1000CDS[2] search engine to compare the miR-124 interactome to signatures of different chemical compounds, including pharmaceuticals, to explore drugs that could be repurposed to reverse or mimic the post-TBI miR-124 interactome. The results with complete information of the 50 top compounds, their mechanism of action, the cell lines, overlapping signature molecules and, if applicable, the disease targeted by the compound (ClinicalTrials.gov) are presented in the supplementary material [Online Resource 2. (reverse) and Online Resource 3. (mimic)]. The compounds with the highest overlap score [0, 1] for reversing the miR-124 interactome after TBI were TW37, importazole, and IKK-16 (Fig. 9a). Respectively, the top three compounds that mimic the miR-124 interactome after TBI were Obatoclax (S1057), torin-1, and ingenol 3,20-dibenzoate (Fig. 9b). Compounds reversing (Fig. 9c) or mimicking (Fig. 9d) the miR-124 interactome after TBI often targeted proliferation, transcription, translation, and protein processing.

Discussion

The present study aimed to identify the mechanisms that maintain chronic transcriptomic changes in the dentate gyrus after TBI. Our bioinformatics analysis suggested that downregulation of brain-enriched miR-124-3p is a master regulator for a set of upregulated genes, even at 3 months post-TBI. Our laboratory validation studies confirmed that miR-124-3p is chronically regulated after TBI in both the experimental animal model and in humans with TBI, as well as in another brain injury model, amygdala stimulation-induced SE. Our data implicate miR-124-3p as a potential treatment target with a wide therapeutic window to combat the evolution of hippocampus-dependent functional impairments after brain injuries.

Chronic downregulation of miR-124-3p after TBI in the dentate gyrus is not related to neurodegeneration

IPA analysis of regulated genes in the dentate gyrus in rats decapitated at 3 months after lateral FPI-induced TBI indicated the upregulation of 30 genes that were miR-124-3p targets. The bioinformatics analysis predicted the downregulation of miR-124-3p at 3 months post-TBI, which was confirmed by ddPCR. Interestingly, Miao et al. [10] showed a downregulation of miR-124-3p in the perilesional cortex at 6 h after controlled cortical impact injury-induced TBI. These findings suggest a wide time window for the downregulation of miR-124-3p and consequent upregulation of its target genes. However, there is still a need for investigation if the level of miR-124-3p is connected to the disease severity and functional outcome.

As lateral FPI results in 10–20% loss of principal cells and up to 50% loss of different types of inhibitory interneurons [39, 41, 54], we next assessed whether

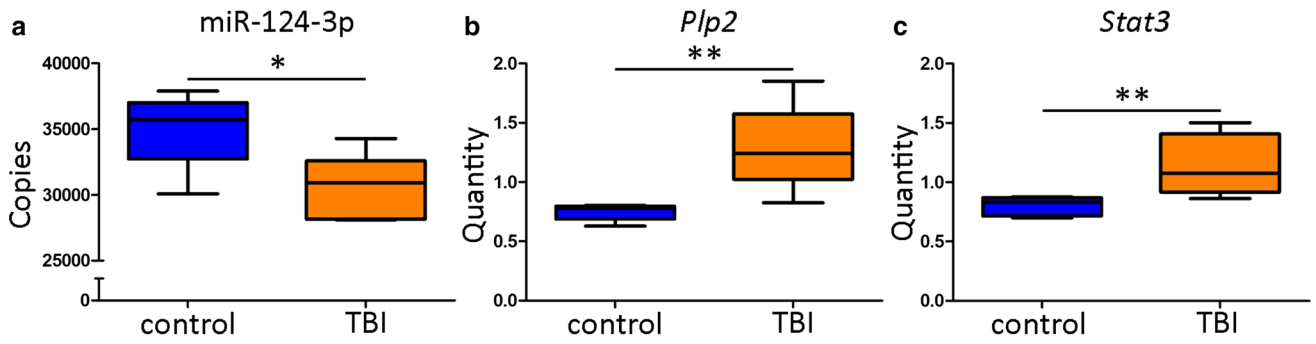

d

Gene	Gene description	Correlation coefficient[1]
Bmp6	bone morphogenetic protein 6	-.752**
C2orf88	chromosome 2 open reading frame 88	-.501
Ccl2	chemokine (C-C motif) ligand 2	-.665*
Cdk6	cyclin-dependent kinase 6	-.696*
Ctdsp1	CTD (carboxy-terminal domain, RNA polymerase II, polypeptide A) small phosphatase 1	-.592
Eci2	enoyl-CoA delta isomerase 2	-.260
Foxq1	forkhead box Q1	-.387
Frmd8	FERM domain containing 8	-.519
Gsn	gelsolin	-.433
Lamc1	laminin, gamma 1	-.460
Limch1	LIM and calponin homology domains 1	-.383
Lrrc57	leucine rich repeat containing 57	.601
Myo10	myosin X	-.817**
Plp2	proteolipid protein 2 (colonic epithelium-enriched)	-.770**
Ppfibp2	PTPRF interacting protein, binding protein 2 (liprin beta 2)	-.438
Prkd1	protein kinase D1	-.478
Prrx1	paired related homeobox 1	-.670*
Ptbp1	polypyrimidine tract binding protein 1	-.510
Rab27a	RAB27A, member RAS oncogene family	-.159
Rbms1	RNA binding motif, single stranded interacting protein 1	-.738**
Rhoj	ras homolog gene family, member J	-.301
Slc7a2	solute carrier family 7 (cationic amino acid transporter, y+ system), member 2	-.352
Stat3	signal transducer and activator of transcription 3	-.596
Swap70	SWAP switching B-cell complex 70	-.632*
Tjp2	tight junction protein 2	-.711*
Tln1	talin 1	-.743**
Tmbim1	transmembrane BAX inhibitor motif containing 1	-.519
Tom1L1	target of myb1 like 1 membrane trafficking protein	-.392
Vat1	vesicle amine transport protein 1 homolog (T californica)	-.747**
Vim	vimentin	-.319
Zfp36l2	zinc finger protein 36, C3H type-like 2	-.551

1: *p<0.05; **p<0.01

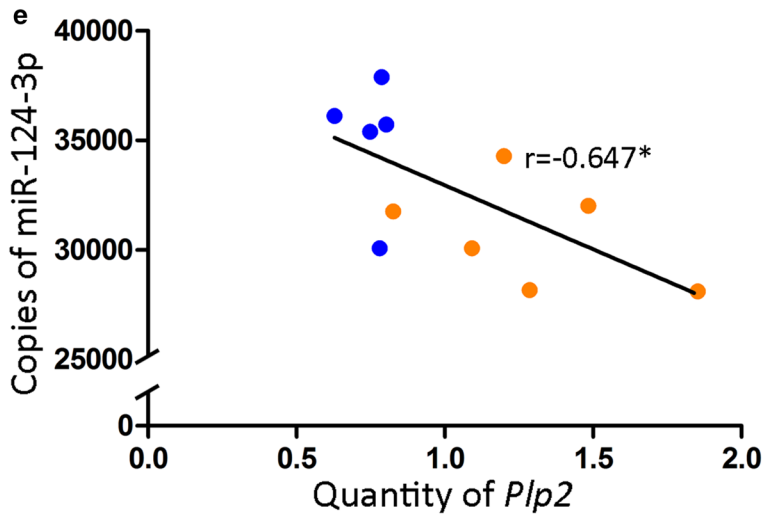

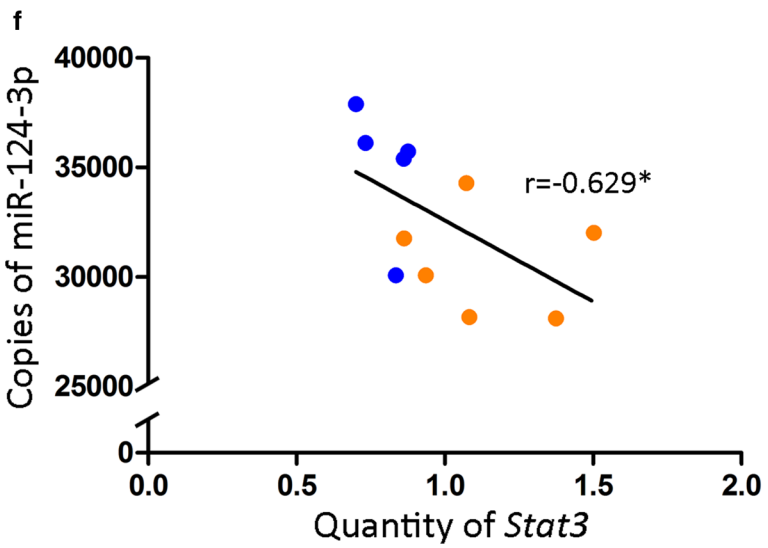

Fig. 3 Wet lab validation of chronic regulation of miR-124-3p and two of its targets after TBI. **a** Droplet digital PCR (ddPCR) analysis of the samples used for the mRNA microarray analysis showed a downregulation of miR-124-3p (FC 0.88, $p<0.05$). Quantitative RT-PCR validation of the gene expression analysis results of two miR-124-3p targets confirmed the upregulation of **b** *Plp2* (FC 1.70, $p<0.01$) and **c** *Stat3* (FC 1.4, $p<0.01$) at 3 months post-TBI. **d** Correlation analysis revealed that upregulation of 11 of the 31 miR-124-3p targets (gene array) correlated with the miR-124-3p downregulation (ddPCR) at 3 months post-TBI. Note that the correlation with *Stat3* expression was not statistically significant. Correlation analysis performed using gene expression measured with qRT-PCR, however, revealed an inverse correlation between the expression of miR-124-3p and **e** *Plp2* ($p<0.05$) as well as with **e** *Stat3* ($p<0.05$). *Plp2* proteolipid protein 2, *r* correlation coefficient, *Stat3* signal transducer and activator of transcription 3, *TBI* traumatic brain injury. Statistical significance: *$p<0.05$, **$p<0.01$ (Mann–Whitney *U*)

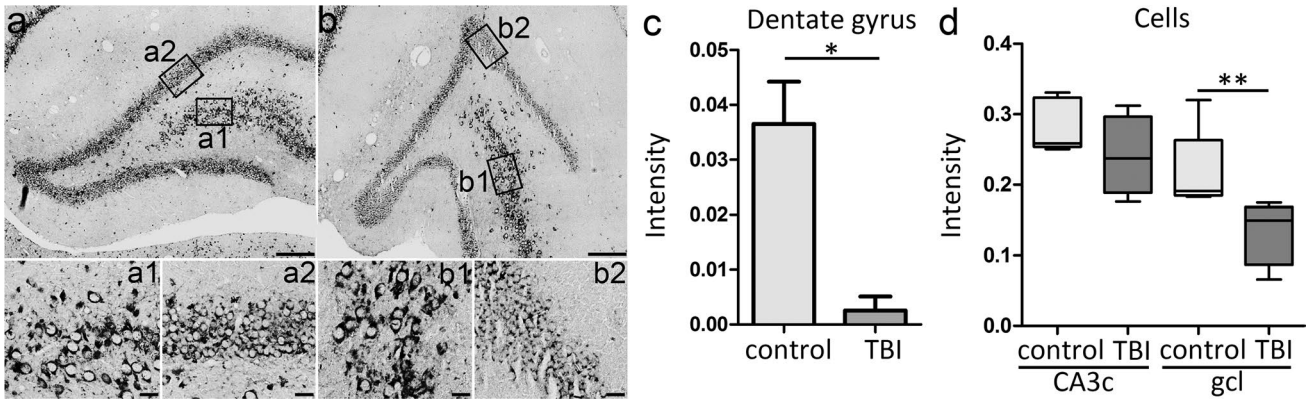

Fig. 4 Intensity analysis of miR-124 in situ hybridization revealed downregulation of miR-124 in neurons of the dentate gyrus after TBI. **a**, **b** Representative photomicrographs of miR-124-3p in situ hybridization (ISH) in the dentate gyrus in a control (**a**) and TBI rat (**b**). Higher magnification images of CA3c and granule cell layers are shown in (a1, b1) and (a2, b2), respectively. **c** Bar graphs show a remarkable reduction in the overall neuronal intensity of miR-124-3p at 3 months post-TBI compared with the control group ($p < 0.05$). **d** As shown in **a** and **b**, the difference between the TBI and control sections was smaller in the CA3c area (b1 vs. a1) than in the granule cell layer (b2 vs. a2). To quantify the differences, we analyzed the mean intensity of in situ hybridization signals in 50 individual cells in CA3c and the granule cell layer from all sections. After TBI, there was a trend toward downregulation of miR-124-3p in neurons in the CA3c area and a robust downregulation in the granule cell layer (**d**, $p < 0.01$). *CA3c* cornu ammonis 3c, *gcl* granule cell layer, *TBI* traumatic brain injury. Scale bar **a**, **b** 500 µm, **a**, **b** 50 µm. Statistical significance $^*p < 0.05$, $^{**}p < 0.01$ (Mann–Whitney *U*)

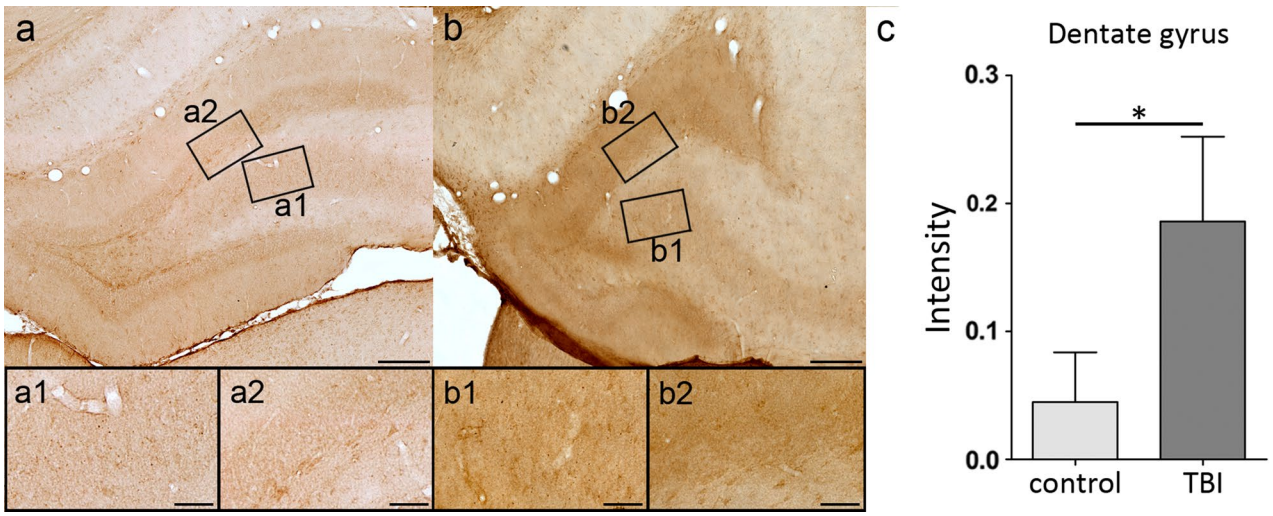

Fig. 5 Chronic upregulation of the miR-124-3p target gene STAT3 after TBI. Representative images from sections of dentate gyrus in a control (**a**) and injured rat (**b**) stained with anti-STAT3 antibody. High-magnification photomicrographs (a1, a2 control, b1, b2 TBI rat) highlight the upregulation of STAT3. Quantitative comparison of the staining intensity between control and TBI animals revealed significant upregulation of STAT3 in the dentate gyrus (**c**, $p < 0.05$). *TBI* traumatic brain injury. Scale bar **a**, **b** 200 µm, **a**, **b** 50 µm. Statistical significance $^*p < 0.05$ (Mann–Whitney *U*)

miR-124-3p downregulation was associated with cell loss in the dentate gyrus rather than regulation of its expression. Previous studies demonstrated that miR-124-3p is consistently expressed in glutamatergic projection neurons as well as in parvalbumin- and somatostatin-positive GABAergic neurons [59]. Our data showed that miR-124-3p is equally downregulated in the excitatory granule cells and parvalbumin-positive interneurons after TBI. Previous analysis of our Affymetrix gene expression array indicated that the granule cell layer is not affected by TBI whereas interneuronal markers are downregulated [36]. Our in situ hybridization analysis revealed downregulation of miR-124 in individual neurons. Furthermore, our analysis of the human dentate gyrus suggests that chronic miR-124 expression is also impaired in patients with TBI, although additional studies are needed to confirm these findings and to identify heterogeneity between patients.

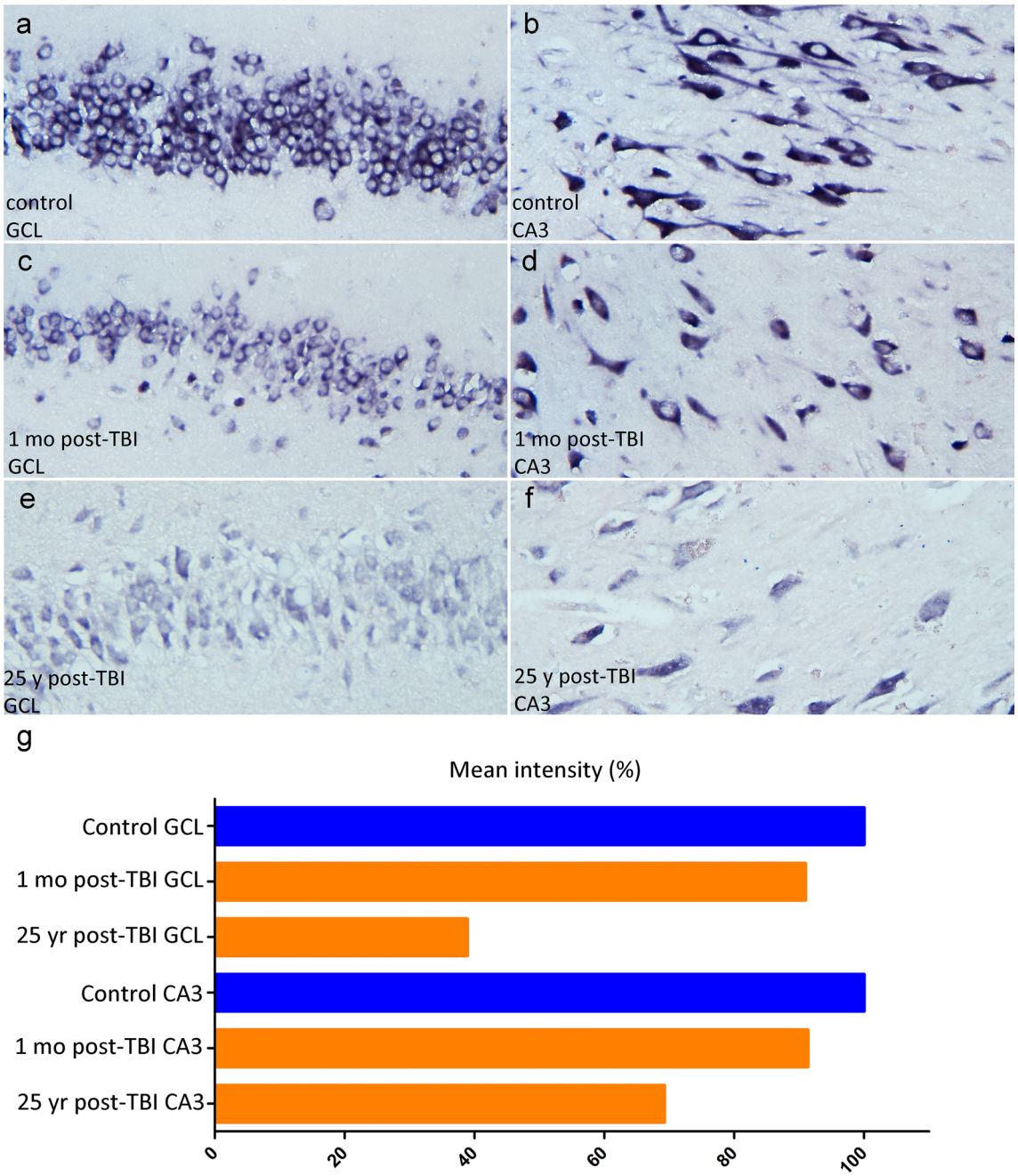

Fig. 6 In situ hybridization of miR-124 in the human dentate gyrus showed chronic post-TBI downregulation of miR-124 in the granule cell layer and CA3. In situ hybridization was performed with human dentate gyrus samples from a patient with no neurologic disorders ($n=5$, **a**, **b**) and a patient that had suffered TBI 1 month (**c**, **d**) or 25 years earlier (**e**, **f**). **g** Analysis of the mean intensity of in situ hybridization revealed downregulation of miR-124 in both the granule cell layer and CA3 of dentate gyrus. *GLC*, granule cell layer, *TBI* traumatic brain injury

Moreover, in our datasets, the pre-miRNA forms of miR-124-3p remained at control levels after TBI and SE (data not shown for SE), indicating that the miR-124-3p reduction was related to reduced maturation of miRNA rather than to cell loss in the dentate gyrus.

Chronic upregulation of miR-124-3p targets after TBI reveals possible function of miR-124-3p in post-injury neurogenesis and the inflammatory response

Text mining of the function of 30 chronically upregulated

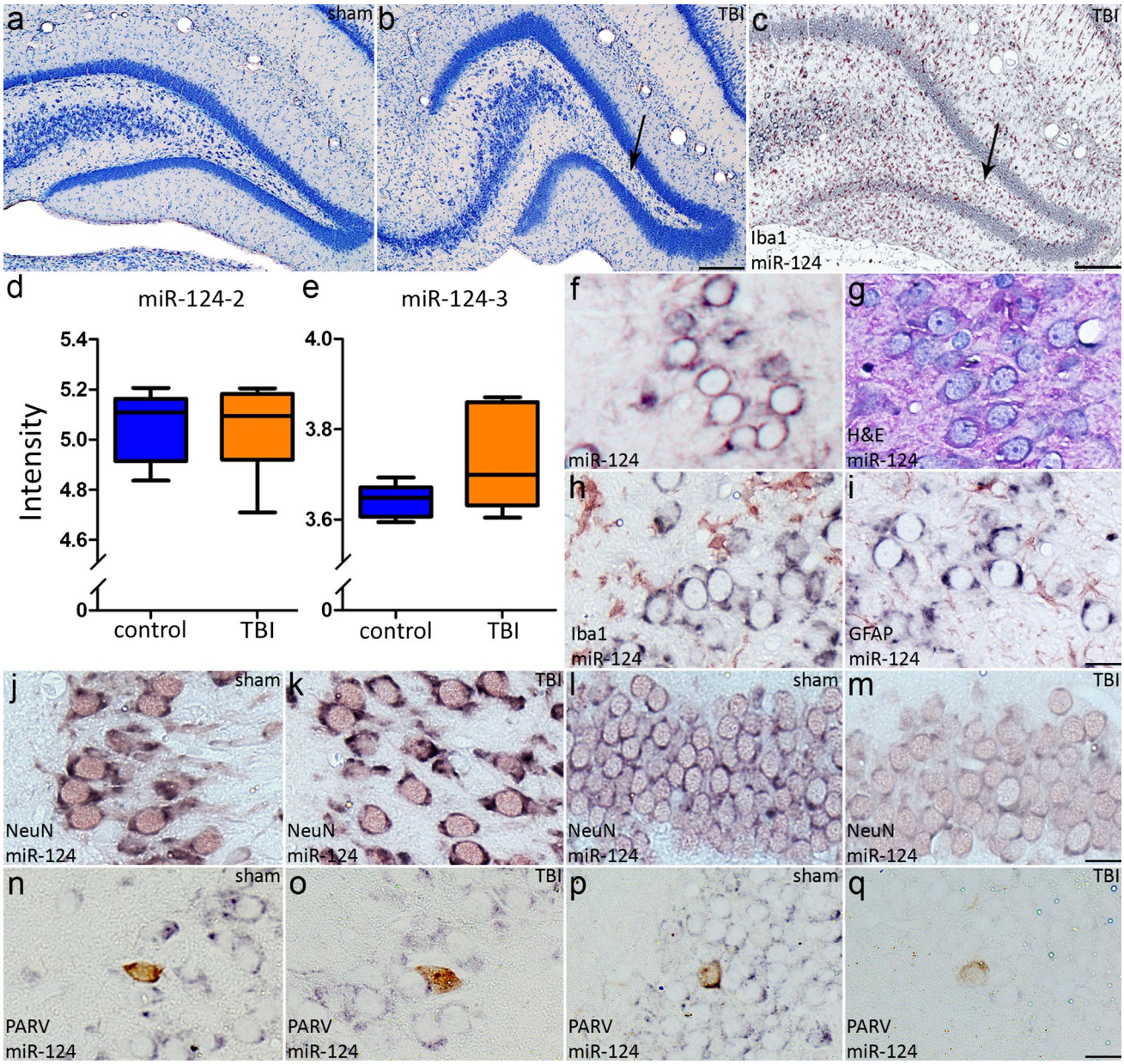

Fig. 7 Post-TBI downregulation of miR-124 is not caused solely by neuronal loss. Lateral fluid-percussion injury results in a loss of hilar cells, as seen in representative photomicrographs of thionin-stained sections of sham-operated control (**a**) and a rat with TBI (**b**, 3 months post-TBI), and notable gliosis, as seen in immunohistologic staining against a microglia marker combined with miR-124 in situ hybridization (gliosis marked with arrows in **b** and **c**). In the transcriptomic profiling data, the expression of two miR-124-3p precursors in the mRNA array (**d**) miR-124-2 or (**e**) miR-124-3, did not differ from that in controls at 3 months post-TBI (both $p > 0.05$), suggesting that neurodegeneration was not the sole cause of the transcription changes. To investigate the cellular location of miR-124-3p, we first performed miR-124 in situ hybridization (example in **f**) together with hematoxylin and eosin (H&E) staining (**g**) or double-labeling with Iba1 (**h**, microglia), GFAP (**i**, astrocytes) or NeuN (**j**–**m**, neurons). These histologic preparations showed that miR-124 is located solely in the cytosol of neurons in both control rats and animals after TBI. Our analysis indicated no change in the miR-124 level in the neurons located in the CA3c (**j**, **k**). However, in the granule cell layer, there was a robust loss of miR-124 intensity (**l**, **m**). To determine if there is difference in the expression of miR-124 in different subtypes of neurons, we conducted miR-124 in situ hybridization together with parvalbumin double-labeling (**n**–**q**). These results indicated that miR-124 is also downregulated in the parvalbumin-positive interneurons located in the granule cell layer of the dentate gyrus. Similar to all NeuN positive neurons, parvalbumin immunoreactive cells located in the CA3c still had evident miR-124 labeling after TBI. *H&E* hematoxylin & eosin, *PARV* parvalbumin, *TBI* traumatic brain injury. Scale bar **a**–**c** 200 µm, **a**, **b** 20 µm

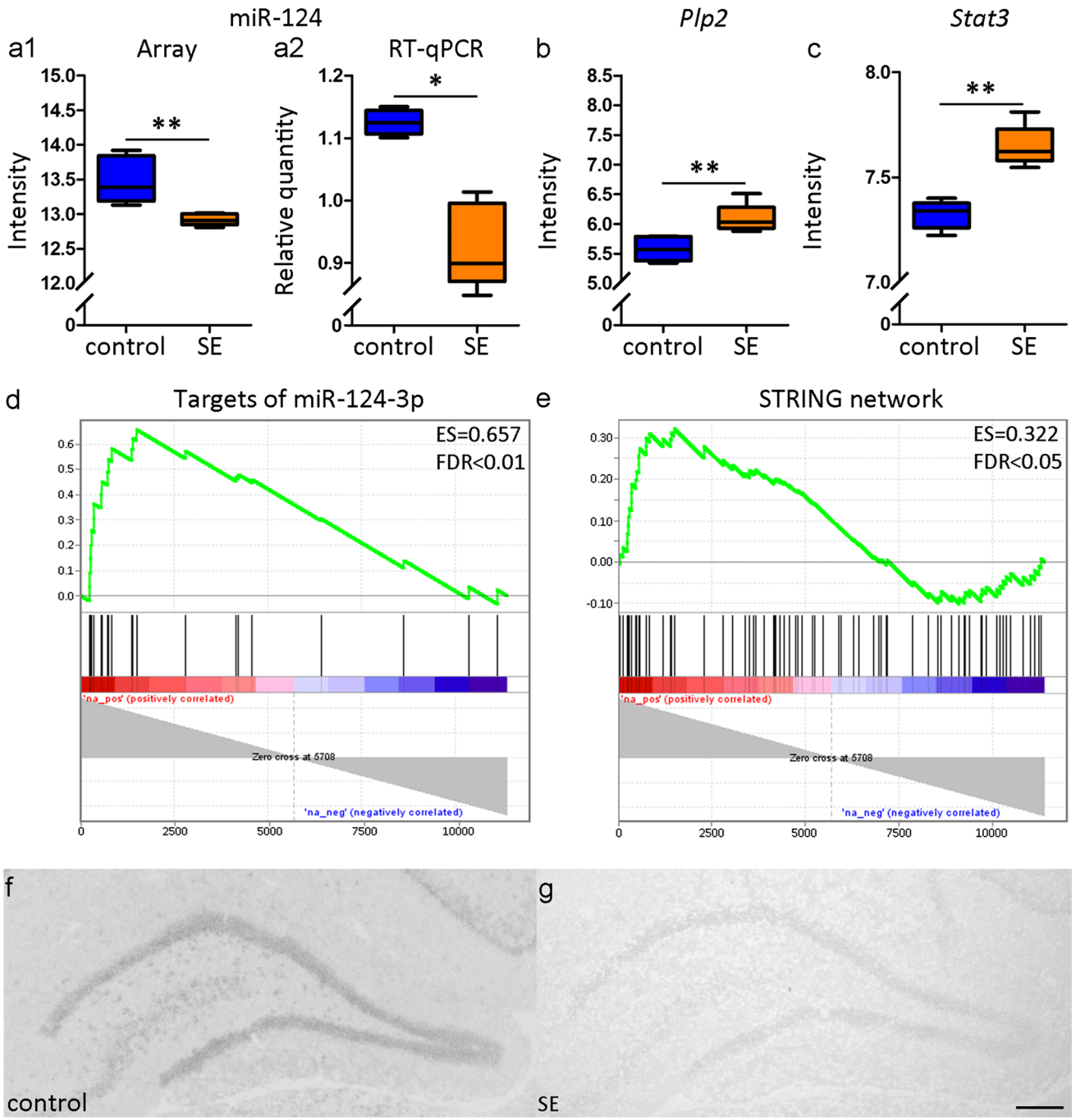

Fig. 8 Regulation of miR-124-3p and its targets 7 days after status epilepticus. **a1** According to microarray gene expression analysis, miR-124-3p expression was decreased at 7 days post-SE ($p < 0.01$). **a2** Further qRT-PCR analysis also revealed downregulation of miR-124-3p ($p < 0.05$). Transcriptomics profiling data (microarray analysis) showed upregulation of two miR-124-3p targets, **b** *Plp2* and **c** *Stat3*. **d** In the GSEA analysis, 15 of 31 miR-124 targets were positively enriched at 7 days post-SE (ES = 0.657, FDR < 0.01). **e** From the molecules in the STRING networks, 76 genes were present in the dataset and 22 of those were enriched (ES = 0.322, FDR < 0.05). In situ hybridization was used to detect miR-124-3p–positive cells. **f**, **g** The color of sections indicates that the control animals have higher miR-124-3p expression levels than SE animals in the dentate gyrus. *ES* enrichment score, *FDR* false discovery rate, *Plp2* proteolipid protein 2, *SE* status epilepticus, *Stat3* signal transducer and activator of transcription 3. Scale bar 50 µm. Statistical significance $*p < 0.05$, $**p < 0.01$ (Mann–Whitney *U*)

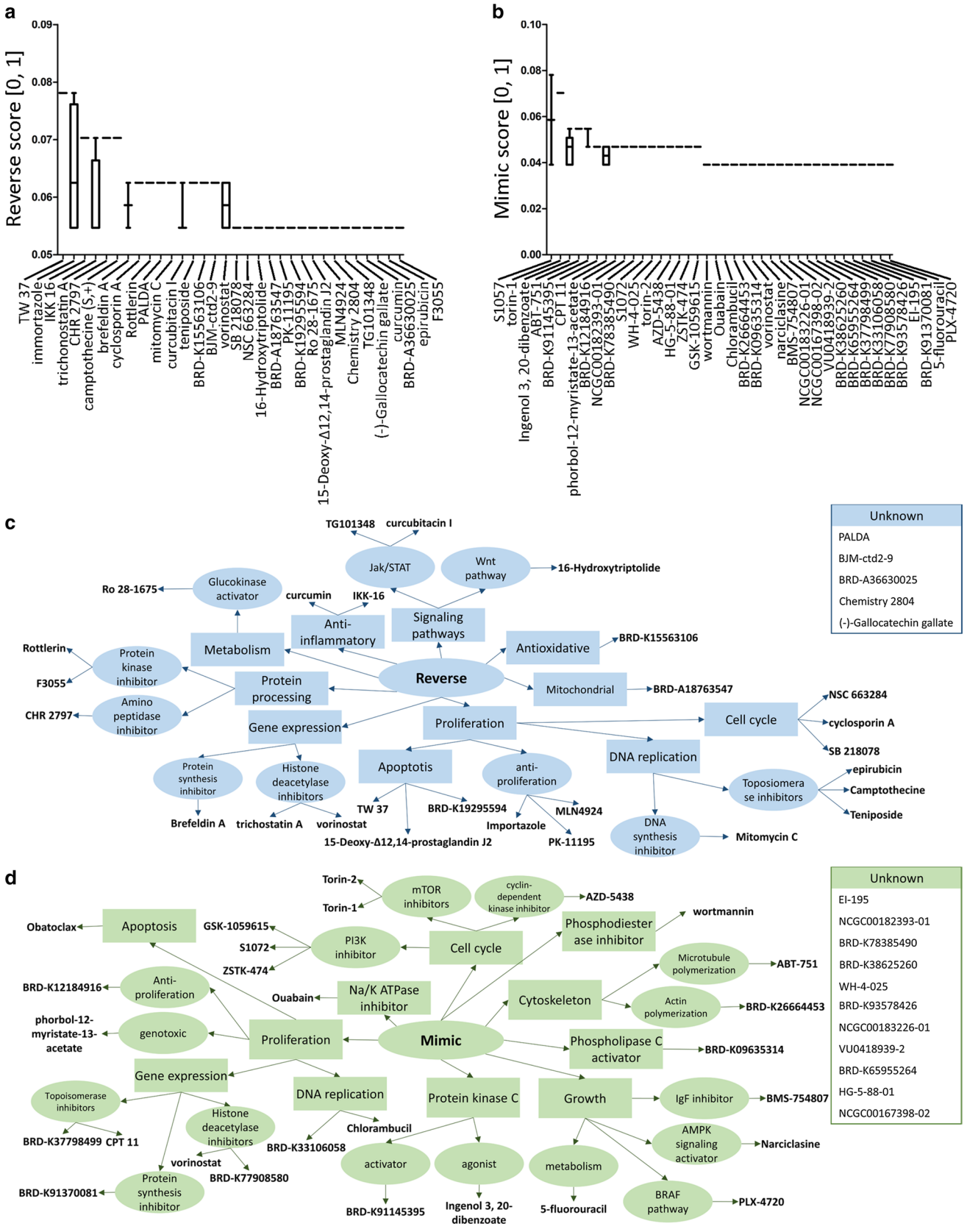
a
Reverse score [0, 1]
0.09
0.08
0.07
0.06
0.05
TW 37
immortazole
IKK 16
trichonostatin A
CHR 2797
camptothecine (S,+)
brefeldin A
cyclosporin A
Rottlerin
PALDA
mitomycin C
curcubitacin I
teniposide
BRD-K15563106
BJM-ctd2-9
vorinostat
SB 218078
NSC 663284
16-Hydroxytriptolide
BRD-A18763547
PK-11195
BRD-K19295594
Ro 28-1675
15-Deoxy-Δ12,14-prostaglandin J2
MLN4924
Chemistry 2804
TG101348
(-)-Gallocatechin gallate
curcumin
BRD-A36630025
epirubicin
F3055
b
Mimic score [0, 1]
0.10
0.08
0.06
0.04
0.02
0.00
S1057
torin-1
Ingenol 3, 20-dibenzoate
ABT-751
BRD-K91145395
CPT 11
phorbol-12-myristate-13-acetate
BRD-K12184916
NCGC00182393-01
BRD-K78385490
S1072
WH-4-025
torin-2
AZD-5438
HG-5-88-01
ZSTK-474
GSK-1059615
wortmannin
Ouabain
Chlorambucil
BRD-K26664453
BRD-K09635314
vorinostat
narciclasine
BMS-754807
NCGC00183226-01
NCGC00167398-02
VU0418939-2
BRD-K38625260
BRD-K65955264
BRD-K37798499
BRD-K33106058
BRD-K77908580
BRD-K93578426
EI-195
BRD-K91370081
5-fluorouracil
PLX-4720
c
Unknown
PALDA
BJM-ctd2-9
BRD-A36630025
Chemistry 2804
(-)-Gallocatechin gallate
TG101348
curcubitacin I
Jak/STAT
Wnt pathway
16-Hydroxytriptolide
Ro 28-1675
Glucokinase activator
curcumin
IKK-16
Anti-inflammatory
Signaling pathways
Rottlerin
Protein kinase inhibitor
Metabolism
Antioxidative
BRD-K15563106
F3055
Reverse
Protein processing
Mitochondrial
BRD-A18763547
CHR 2797
Amino peptidase inhibitor
Gene expression
Proliferation
Cell cycle
NSC 663284
cyclosporin A
SB 218078
Protein synthesis inhibitor
Histone deacetylase inhibitors
Apoptotis
anti-proliferation
DNA replication
Toposiomerase inhibitors
epirubicin
Camptothecine
Teniposide
Brefeldin A
trichostatin A
vorinostat
TW 37
BRD-K19295594
MLN4924
Importazole
PK-11195
15-Deoxy-Δ12,14-prostaglandin J2
DNA synthesis inhibitor
Mitomycin C
d
Unknown
EI-195
NCGC00182393-01
BRD-K78385490
BRD-K38625260
WH-4-025
BRD-K93578426
NCGC00183226-01
VU0418939-2
BRD-K65955264
HG-5-88-01
NCGC00167398-02
Torin-2
Torin-1
mTOR inhibitors
cyclin-dependent kinase inhibitor
AZD-5438
Obatoclax
Apoptosis
GSK-1059615
S1072
ZSTK-474
PI3K inhibitor
Cell cycle
Phosphodiesterase inhibitor
wortmannin
Microtubule polymerization
ABT-751
BRD-K12184916
Anti-proliferation
Ouabain
Na/K ATPase inhibitor
Cytoskeleton
Actin polymerization
BRD-K26664453
phorbol-12-myristate-13-acetate
genotoxic
Proliferation
Mimic
Phospholipase C activator
BRD-K09635314
Gene expression
Topoisomerase inhibitors
DNA replication
Protein kinase C
Growth
IgF inhibitor
BMS-754807
BRD-K37798499
CPT 11
Histone deacetylase inhibitors
Chlorambucil
BRD-K33106058
AMPK signaling activator
Narciclasine
vorinostat
BRD-K77908580
activator
agonist
metabolism
BRAF pathway
PLX-4720
BRD-K91370081
Protein synthesis inhibitor
BRD-K91145395
Ingenol 3, 20-dibenzoate
5-fluorouracil

◂**Fig. 9** L1000CDS2 search of chemical compounds reversing or mimicking the miR-124 interactome emphasizes the complexity of miR-124 controlled pathways. The L1000 Characteristic Direction Signature Search Engine was used to compare the miR-124 interactome and expression profile that chemical compounds invoke in different human cell lines to find drugs that could either reverse (**a**) or mimic (**b**) the miR-124 interactome. **c** PubChem database searches revealed that mechanisms of actions for compounds reversing the TBI-induced miR-124 interactome were most commonly related to proliferation and gene expression. Mimics for the TBI-induced miR-124 interactome were connected to, e.g., growth and gene expression

miR-124-3p targets highlighted the role of miR-124 in inflammation and proliferation. More detailed data mining indicated that these targets regulate several TBI-related secondary pathologies, particularly neurogenesis (BMP6, CTDSP1, CDK6, PTBP1, GSN, MYO10, and STAT3) and neuroinflammation (CCL2, CDK6, and STAT3).

At 3 months post-TBI, CTDSP1 remained upregulated 1.16-fold. CTDSP1 is a nuclear phosphatase that stabilizes RE1-silencing transcription factor (REST; also known as neuron-restrictive silencer factor, NRSF; [60]), allowing it to function as a suppressor of neuron-specific gene expression [61–65]. Similarly, another target of REST, BMP6, was upregulated 1.24-fold. BMP6 is a bone morphogenetic protein that reduces cell proliferation in neural stem cells [66]. REST maintains the pluripotency of embryonic stem cells, as when REST targets are activated, stem cells and even myoblasts can convert to neurons [67–69]. To our knowledge, there are no data on CTDSP1 or REST expression in experimental or human TBI. Previous studies, however, revealed an up to two- to threefold increase in the expression of REST after kainate-induced brain injury [70]. BMP6 levels are increased in the peripheral blood at 3 days after lateral FPI [71]. Whether upregulation of CTDSP1 and BPM6 is needed for post-injury stabilization of increased REST levels, and whether the upregulation is related to miR-124-3p downregulation, however, remain to be explored.

Cyclin-dependent kinase 6 (CDK6) was also upregulated 1.16-fold at 3 months post-TBI. CDK6 is a member of the Cdk family of proteins that regulate cell cycle progression [72]. Cdk6 is expressed in the dentate and subventricular precursor cells, but not in post-mitotic neurons [73]. In the dentate gyrus of $Cdk6^{-/-}$ mice, neuronally committed precursors exhibit a lengthened G1 phase and exit the cell cycle prematurely, indicating that Cdk6 specifically regulates adult neurogenesis [73].

Polypyrimidine tract binding (PTB) proteins are proposed to regulate cell-type specific splicing [74]. Here we demonstrated that PTBP1 was upregulated 1.13-fold at 3 months post-TBI. Previous studies reported that PTBP1 binds to pyrimidine-rich exon sequences of pre-mRNAs, and consequently inhibits splicing of closely located neuron-specific exons [75]. PTBP1 is expressed in most mammalian tissues [76]. In normal brain, however, PTBP1 is replaced by its paralogous protein, PTBP2 [77]. PTBP2 is highly expressed in proliferating and post-mitotic neurons where its main role is to prevent the expression of exons [78]. Interestingly, PTBP1 and PTBP2 counteract each other's functions via competitive binding to pre-mRNA, resulting in a change in its codons, and consequently, a nonsense-mediated decay [79, 80]. In CAD and Neuro2a neuroblastoma cell lines, overexpression of miR-124-3p suppresses PTBP1 expression, which promotes PTBP2-mediated neuron-specific splicing [81]. These studies suggest that the PTBP1/PTBP2 interaction forms a miR-124-3p-dependent post-transcriptional switch for neuronal differentiation [78, 79, 81]. Our data suggest that such a switch, favoring the dominance of PTBP1, could also be operational after TBI.

Finally, we also found a 1.12-fold increase in STAT3 expression with the array and a 1.4-fold upregulation with qRT-PCR at 3 months post-TBI. In addition, our immunohistochemical analysis at 3 months post-TBI also confirmed the upregulation of STAT3 protein. Induction of STAT3 signaling is crucial for forming and preserving the subgranular zone in the dentate gyrus, as adult mice with conditional STAT3 knock-out in neural stem cells exhibit impaired proliferation and neurogenesis in the dentate gyrus [82]. Interestingly, the level of active phosphorylated STAT3 is increased two- to threefold between 6 and 24 h after induction of lateral FPI [56], and normalizes within a week [57]. STAT3 is mainly localized in the nuclei of reactive astrocytes [56]. Most interestingly, Grabenstatter et al. [83] showed that administering a propenamide analog, WP1066, which is a weak inhibitor of the Jak/STAT pathway, reduces the frequency and severity of spontaneous seizures developing after pilocarpine-induced brain injury. They also reported that WP1066 alleviates a decrease in GABA(A) R α1 protein levels after controlled cortical impact (CCI)-induced TBI. Furthermore, WP1066 treatment improved the degree of recovery of vestibular motor function after CCI injury. It remains to be tested whether miR-124-3p upregulation will show favorable disease-modifying effects on post-TBI secondary damage via the STAT3 pathway.

Two of the upregulated miR-124-3p targets, GSN and Myo10, have not been directly linked to neurogenesis. Mice deficient in the extracellular protein GSN, however, exhibit impaired migration of adult neuronal progenitors from the subventricular zone to the olfactory bulb [84]. Interestingly, Myo10 regulates microtubule stability during neuronal development and is critical for axonal development and outgrowth [85–87]. As both axonal injury-related microtubular disorganization and axonal growth are hallmarks of TBI-associated pathology, our data are consistent with studies suggesting a role for miR-124-3p in axonal repair and plasticity [88–90].

In addition to neurogenesis, 3 of the 30 upregulated miR-124-3p targets contribute to the post-injury inflammatory response. CCL2 is a widely studied chemokine that induces angiogenesis through activation of the Ets-1 transcription factor [91]. Ccl2 mediates its signal by binding to the chemokine C–C motif receptor 2 (CCR2), which regulates brain infiltration by monocytes (for a review, see Chu et al. [92]). In mice with mild lateral FPI, deletion of Ccr2 reduces the acute lesion volume and axonal damage, but also increases tau mislocation in the cortex and hippocampus [93]. CDK6 promotes expression of the inflammation-related transcription factors NF-κB and AP-1 (in HeLa cells, [94, 95]) as well as STAT families (B cells, [96]). STAT3, in turn, induces the expression of pro-inflammatory genes [97, 98]. STAT3 is a transcription factor that translocated to the nucleus after induction of an inflammatory response by lipopolysaccharide injection [99]. Thus, our data suggest that downregulation of miR-124-3p contributes to post-TBI inflammation through a consequent increase in STAT3.

To summarize, upregulation of many neuronal miR-124-3p targets either directly or indirectly facilitates the astrocytic fate of progenitor cells in the subgranular zone of the dentate gyrus during neurogenesis. Another TBI-relevant pathology relates to the induction and maintenance of inflammation through the Jak/STAT pathway. Several studies in rodents and humans revealed enriched miR-124-3p in the brain tissue [100–102]. The neuron specificity of miR-124-3p was initially demonstrated in in vitro studies of human primary cultured cells [102], and confirmed by in vivo studies of tissue samples from mice, rats, and humans [103, 104].

Consistent with previous studies, our in situ hybridization analysis of miR-124-3p revealed its neuronal expression in the dentate gyrus both in controls and in rats with TBI, as well as in human hippocampus (data not shown). As some of the functions assigned to miR-124-3p appear to be in astrocytes, it is interesting to note that miR-124-3p is transported through gap junctions to adjacent U87 and C6 glioblastoma cells [105]. Moreover, miR-124-3p is also found in exosomes, which could explain why neuronally expressed miR-124-3p can regulate gene expression in non-neuronal cells [106].

miR-124-3p and its targets in different brain injury models

According to our study, miR-124-3p targets were also upregulated at 7 days after amygdala stimulation-induced SE. In the SE model, the upregulation of miR-124-3p targets is associated with the downregulation of miR-124-3p at 7 days [43]. Our data are consistent with the observations of Gorter et al. [107] that miR-124-3p is downregulated in the dentate gyrus at acute (1 day and 1 week post-SE) time points in a perforant pathway stimulation model of SE. In a systemic pilocarpine model of SE; however, hippocampal miR-124-3p levels are elevated at 24 h post-SE, suggesting some injury-type specificity [108].

In addition to the previously mentioned genes, we found that C2orf88, Foxq1, Frmd8, Plp2, Ppfibp2, Rab27a, Rhoj, Slc7a2, Tjp2, Tln1, Tmbim1, Vim, and Vat1 were upregulated, and Lrrc57 was downregulated. Vim was found to be upregulated at 24 h after blast-induced TBI in rats [109] and deiminated at 2 weeks after blast injury in swine [110]. To our knowledge, a connection between the remaining genes and brain injury has not been demonstrated. Nevertheless, Foxq1 promotes glioma proliferation [111], Rab27a promotes exosome secretion [112], and Rhoj is crucial for endothelial cell formation [113]. Plp2-deficient mice are more prone to endoplasmic reticulum stress, which increases the risk for neonatal hypoxia–ischemia encephalopathy [114]. Our data indicate uncharted functions of miR-124-3p, whose dysregulation could contribute to TBI pathology.

Analysis of the miR-124 interactome reveals novel compounds to combat TBI-induced hippocampal pathologies

The fact that one miRNA can regulate hundreds of mRNAs makes miRNAs attractive treatment targets, but the sheer number of possible targets makes it difficult to predict the outcome of changes to miRNA function. Thus, it might be beneficial to study pharmaceutical compounds that could be used to target a specific pathway to either support or dampen the effect of a miRNA. Our analysis with L1000CDS2 software indicated that the miR-124 interactome has a role in proliferative functions. Furthermore, miR-124 regulates gene expression through histone modifications.

The three compounds with the highest overlap score for reversing the miR-124 interactome suppress proliferation. TW-37 inhibits the anti-apoptotic BCL-2 family of proteins [115]. Importazole, an anti-proliferative drug that inhibits transport receptor importin-β [116], has a key role in transporting proteins to the nucleus [117] and is crucial for mitosis [118]. IKK-16 is an IkB kinase inhibitor that suppresses the NF-kB signal transduction cascade, thereby reducing lymphocyte proliferation and growth, which modulates the immune response [119]. Overall, the analysis highlights drugs known to affect proliferation (PK-11195, importazole, and MLN4924), DNA replication (topoisomerase inhibitors teniposide, camptothecin, and epirubicin), or to arrest the cell cycle (NSC 663284, cyclosporine A, SB218078), suggesting that miR-124 also restricts cell multiplication. PK-11195, a benzodiazepine receptor ligand, disturbs cancer cell proliferation in vitro [120–122]. PK-11195, however, is also used as a tracer of microglial function [123]. In addition, two histone deacetylase I and II inhibitors, vorinostat

and trichostatin A, came up multiple times in different cell lines (4/50 and 9/50, respectively). Increased acetylation of histones leads to altered gene expression. Both drugs induce cell cycle arrest and apoptosis in cancer cells [124–128].

Interestingly, the top compound to mimic the miR-124 interactome, obatoclax, is a Bcl-2 inhibitor and thus pro-apoptotic [129]. The other major regulators were torin-1 and Ingenol 3,20-dibenzoate. Torin-1 directly targets mTOR (mechanistic target of rapamycin) [130]. Inactivation of mTOR promotes autophagy and induces apoptosis in cancer cells [131, 132]. Studies using a mouse CCI model revealed that treatment with an mTOR inhibitor reduces synaptic reorganization of granule cells, which could lead to the development of spontaneous seizures [133, 134]. Everolimus, an mTOR inhibitor, decreased the volume of a subependymal giant cell astrocytoma and inhibited epileptogenesis associated with tuberous sclerosis [135–137]. Ingenol 3,20-dibenzoate is protein kinase C agonist [138] that in turn inhibits autophagy [139].

The list of "mimicking" drugs includes several compounds, such as histone deacetylase inhibitors and topoisomerase inhibitors that are also present in "reversing" pathways. This highlights the complexity of miRNA-controlled pathways, and supports the idea of using big data to search for tailored compounds to target only limited beneficial cellular functions.

Conclusions

miR-124-3p is chronically downregulated and its targets upregulated in the dentate gyrus in two clinically relevant brain injury models, TBI and SE, as well as in human TBI patients. Whether downregulation of miR-124-3p is pathological or compensatory mechanism after brain injuries remains to be studied. We identified 30 chronically upregulated miR-124-3p targets known to contribute to post-injury cellular pathologies. We propose that these target genes could serve as novel treatment targets for brain injuries. Our bioinformatics analysis predicted importazole, trichostatin A, and IKK-16 as top candidate compounds to reverse miR-124-3p-dependent gene expression regulation after TBI. Proof-of-concept in vivo studies in animal models of TBI and SE demonstrated that inhibition of one of the miR-124-3p targets, STAT3, by WP1066 improves post-TBI recovery [57, 75]. Despite this small piece of evidence, more studies are needed to determine whether inhibition of miR-124 targets could benefit treatment of post-TBI pathologies.

Acknowledgements The research leading to these results received funding from the Academy of Finland (AP) Grant nos. (272249, 273909), Polish National Science Centre Grants (2015/16/T/NZ4/00175 and 2014/15/N/NZ4/04561), as well as from the European Union's Seventh Framework Programme (FP7/2007–2013) under Grant agreement n°602102 (EPITARGET). We acknowledge the technical support generously provided by Mr. Jarmo Hartikainen, Mrs. Merja Lukkari, and Mr. Jasper Anink.

References

1. Langlois JA, Rutland-Brown W, Wald MM (2006) The epidemiology and impact of traumatic brain injury: a brief overview. J Head Trauma Rehabil 21(5):375–378
2. Wong VS, Langley B (2016) Epigenetic changes following traumatic brain injury and their implications for outcome, recovery and therapy. Neurosci Lett 625:26–33
3. Rola R, Mizumatsu S, Otsuka S, Morhardt DR, Noble-Haeusslein LJ, Fishman K et al (2006) Alterations in hippocampal neurogenesis following traumatic brain injury in mice. Exp Neurol 202(1):189–199
4. Lee RC, Ambros V (2001) An extensive class of small RNAs in *Caenorhabditis elegans*. Science 294(5543):862–864
5. Lee RC, Feinbaum RL, Ambros V (1993) The *C. elegans* heterochronic gene lin-4 encodes small RNAs with antisense complementarity to lin-14. Cell 75(5):843–854
6. Bartel DP (2004) MicroRNAs: genomics, biogenesis, mechanism, and function. Cell 116(2):281–297
7. Liu L, Sun T, Liu Z, Chen X, Zhao L, Qu G et al (2014) Traumatic brain injury dysregulates MicroRNAs to modulate cell signaling in rat hippocampus. PLoS One 9(8):e103948
8. Sandhir R, Gregory E, Berman NEJ (2014) Differential response of miRNA-21 and its targets after traumatic brain injury in aging mice. Neurochem Int 78:117–121
9. Sabirzhanov B, Zhao Z, Stoica BA, Loane DJ, Wu J, Borroto C et al (2014) Downregulation of miR-23a and miR-27a following experimental traumatic brain injury induces neuronal cell death through activation of proapoptotic Bcl-2 proteins. J Neurosci 34(30):10055–10071
10. Miao W, Bao TH, Han JH, Yin M, Yan Y, Wang WW et al (2015) Voluntary exercise prior to traumatic brain injury alters miRNA expression in the injured mouse cerebral cortex. Braz J Med Biol Res 48(5):433–439
11. Wang W, Visavadiya NP, Pandya JD, Nelson PT, Sullivan PG, Springer JE (2015) Mitochondria-associated microRNAs in rat hippocampus following traumatic brain injury. Exp Neurol 265:84–93
12. Bao T, Miao W, Han J, Yin M, Yan Y, Wang W et al (2014) Spontaneous running wheel improves cognitive functions of mouse associated with miRNA expressional alteration in hippocampus following traumatic brain injury. J Mol Neurosci 54(4):622–629
13. Meissner L, Gallozzi M, Balbi M, Schwarzmaier S, Tiedt S, Terpolilli NA et al (2016) Temporal profile of microRNA expression in contused cortex after traumatic brain injury in mice. J Neurotrauma 33(8):713–720
14. Valiyaveettil M, Alamneh YA, Miller S-, Hammamieh R, Arun P, Wang Y et al (2013) Modulation of cholinergic pathways and inflammatory mediators in blast-induced traumatic brain injury. Chem Biol Interact 203(1):371–375
15. Wang Y, Guo F, Pan C, Lou Y, Zhang P, Guo S et al (2012) Effects of low temperatures on proliferation-related signaling pathways in the hippocampus after traumatic brain injury. Exp Biol Med 237(12):1424–1432
16. Truettner JS, Alonso OF, Bramlett HM, Dietrich WD (2011) Therapeutic hypothermia alters microRNA responses to traumatic brain injury in rats. J Cereb Blood Flow Metab 31(9):1897–1907

17. Truettner JS, Motti D, Dietrich WD (2013) MicroRNA overexpression increases cortical neuronal vulnerability to injury. Brain Res 1533:122–130
18. Hu Z, Yu D, Almeida-Suhett C, Tu K, Marini AM, Eiden L et al (2012) Expression of miRNAs and their cooperative regulation of the pathophysiology in traumatic brain injury. PLoS One 7(6):e39357
19. Redell JB, Liu Y, Dash PK (2009) Traumatic brain injury alters expression of hippocampal microRNAs: potential regulators of multiple pathophysiological processes. J Neurosci Res 87(6):1435–1448
20. Redell JB, Zhao J, Dash PK (2011) Altered expression of miRNA-21 and its targets in the hippocampus after traumatic brain injury. J Neurosci Res 89(2):212–221
21. Sharma A, Chandran R, Barry ES, Bhomia M, Hutchison MA, Balakathiresan NS et al (2014) Identification of serum MicroRNA signatures for diagnosis of mild traumatic brain injury in a closed head injury model. PLoS One 9(11):e112019
22. Schober K, Ondruschka B, Dreßler J, Abend M (2015) Detection of hypoxia markers in the cerebellum after a traumatic frontal cortex injury: a human postmortem gene expression analysis. Int J Leg Med 129(4):701–707
23. Balakathiresan N, Bhomia M, Chandran R, Chavko M, McCarron RM, Maheshwari RK (2012) MicroRNA let-7i is a promising serum biomarker for blast-induced traumatic brain injury. J Neurotrauma 29(7):1379–1387
24. Taheri S, Tanriverdi F, Zararsiz G, Elbuken G, Ulutabanca H, Karaca Z et al (2016) Circulating microRNAs as potential biomarkers for traumatic brain injury-induced hypopituitarism. J Neurotrauma 33(20):1818–1825
25. Redell JB, Moore AN, Ward NH, Hergenroeder GW, Dash PK (2010) Human traumatic brain injury alters plasma microRNA levels. J Neurotrauma 27(12):2147–2156
26. You W, Tang Q, Wang L, Lei J, Feng J, Mao Q et al (2016) Alteration of microRNA expression in cerebrospinal fluid of unconscious patients after traumatic brain injury and a bioinformatic analysis of related single nucleotide polymorphisms. Chin J Traumatol Eng Ed 19(1):11–15
27. Ge X, Lei P, Wang H, Zhang A, Han Z, Chen X et al (2014) MiR-21 improves the neurological outcome after traumatic brain injury in rats. Sci Rep 4:6718. https://doi.org/10.1038/srep06718
28. Ge X, Han Z, Chen F, Wang H, Zhang B, Jiang R et al (2015) MiR-21 alleviates secondary blood–brain barrier damage after traumatic brain injury in rats. Brain Res 1603:150–157
29. Jadhav SP, Kamath SP, Choolani M, Lu J, Dheen ST (2014) MicroRNA-200b modulates microglia-mediated neuroinflammation via the cJun/MAPK pathway. J Neurochem 130(3):388–401
30. Han Z, Chen F, Ge X, Tan J, Lei P, Zhang J (2014) MiR-21 alleviated apoptosis of cortical neurons through promoting PTEN-Akt signaling pathway in vitro after experimental traumatic brain injury. Brain Res 1582:12–20
31. Sabirzhanov B, Stoica BA, Zhao Z, Loane DJ, Wu J, Dorsey SG et al (2016) MiR-711 upregulation induces neuronal cell death after traumatic brain injury. Cell Death Differ 23(4):654–668
32. Hu T, Zhou F-, Chang Y-, Li Y-, Liu G-, Hong Y et al (2015) miR21 is associated with the cognitive improvement following voluntary running wheel exercise in TBI mice. J Mol Neurosci 57(1):114–122
33. Owen DR, Narayan N, Wells L, Healy L, Smyth E, Rabiner EA et al (2017) Pro-inflammatory activation of primary microglia and macrophages increases 18 kDa translocator protein expression in rodents but not humans. J Cereb Blood Flow Metab 37(8):2679–2690
34. Johansson S, Lee I-, Olson L, Spenger C (2005) Olfactory ensheathing glial co-grafts improve functional recovery in rats with 6-OHDA lesions. Brain 128(12):2961–2976
35. Ramlackhansingh AF, Brooks DJ, Greenwood RJ, Bose SK, Turkheimer FE, Kinnunen KM et al (2011) Inflammation after trauma: microglial activation and traumatic brain injury. Ann Neurol 70(3):374–383
36. Puhakka N, Bot AM, Vuokila N, Debski KJ, Lukasiuk K, Pitkänen A (2017) Chronically dysregulated NOTCH1 interactome in the dentate gyrus after traumatic brain injury. PLoS One 12(3):e0172521
37. Sun D (2016) Endogenous neurogenic cell response in the mature mammalian brain following traumatic injury. Exp Neurol 275(Pt 3):405–410. https://doi.org/10.1016/j.expneurol.2015.04.017 **(Epub 2015 Apr 30)**
38. Faden AI, Wu J, Stoica BA, Loane DJ (2016) Progressive inflammation-mediated neurodegeneration after traumatic brain or spinal cord injury. Br J Pharmacol 173(4):681–691. https://doi.org/10.1111/bph.13179 **(Epub 2015 Jun 12)**
39. Huusko N, Römer C, Ndode-Ekane XE, Lukasiuk K, Pitkänen A (2013) Loss of hippocampal interneurons and epileptogenesis: a comparison of two animal models of acquired epilepsy. Brain Struct Funct 220(1):153–191
40. McIntosh TK, Vink R, Noble L, Yamakami I, Fernyak S, Soares H, Faden AL (1989) Traumatic brain injury in the rat: characterization of a lateral fluid-percussion model. Neuroscience 28:233–244
41. Kharatishvili I, Nissinen JP, McIntosh TK, Pitkänen A (2006) A model of posttraumatic epilepsy induced by lateral fluid-percussion brain injury in rats. Neuroscience 140(2):685–697
42. Nissinen J, Halonen T, Koivisto E, Pitkänen A (2000) A new model of chronic temporal lobe epilepsy induced by electrical stimulation of the amygdala in rat. Epilepsy Res 38(2–3):177–205
43. Bot AM, Debski KJ, Lukasiuk K (2013) Alterations in miRNA levels in the dentate gyrus in epileptic rats. PLoS One 8(10):e76051
44. Paxinos G, Watson C (2007) The rat brain in stereotaxic coordinates, 6th edn. Elsevier, Amsterdam
45. Pitkänen A, Kharatishvili I, Karhunen H, Lukasiuk K, Immonen R, Nairismägi J et al (2007) Epileptogenesis in experimental models. Epilepsia 48(SUPPL. 2):13–20
46. Szklarczyk D, Franceschini A, Wyder S, Forslund K, Heller D, Huerta-Cepas J et al (2015) STRING v10: protein–protein interaction networks, integrated over the tree of life. Nucleic Acids Res 43(D1):D447–D452
47. Shannon P, Markiel A, Ozier O, Baliga NS, Wang JT, Ramage D et al (2003) Cytoscape: a software environment for integrated models of biomolecular interaction networks. Genome Res 13(11):2498–2504
48. Subramanian A, Tamayo P, Mootha VK, Mukherjee S, Ebert BL, Gillette MA et al (2005) Gene set enrichment analysis: a knowledge-based approach for interpreting genome-wide expression profiles. Proc Natl Acad Sci USA 102(43):15545–15550
49. Mootha VK, Lindgren CM, Eriksson K-, Subramanian A, Sihag S, Lehar J et al (2003) PGC-1α-responsive genes involved in oxidative phosphorylation are coordinately downregulated in human diabetes. Nat Genet 34(3):267–273
50. Fabregat A, Sidiropoulos K, Garapati P, Gillespie M, Hausmann K, Haw R et al (2016) The reactome pathway knowledgebase. Nucleic Acids Res 44(D1):D481–D487
51. Croft D, Mundo AF, Haw R, Milacic M, Weiser J, Wu G et al (2014) The reactome pathway knowledgebase. Nucleic Acids Res 42(D1):D472–D477
52. Miotto E, Saccenti E, Lupini L, Callegari E, Negrini M, Ferracin M (2014) Quantification of circulating miRNAs by droplet digital PCR: comparison of EvaGreen- and TaqMan-based chemistries. Cancer Epidemiol Biomark Prev 23(12):2638–2642

53. Lewis DA, Campbell MJ, Morrison JH (1986) An immunohistochemical characterization of somatostatin-28 and somatostatin-$28_{1–12}$ in monkey prefrontal cortex. J Comp Neurol 248(1):1–18
54. Grady MS, Charleston JS, Maris D, Witgen BM, Lifshitz J (2003) Neuronal and glial cell number in the hippocampus after experimental traumatic brain injury: analysis by stereological estimation. J Neurotrauma 20(10):929–941
55. Cai B, Li J, Wang J, Luo X, Ai J, Liu Y, Wang N, Liang H, Zhang M, Chen N, Wang G, Xing S, Zhou X, Yang B, Wang X, Lu Y (2012) MicroRNA-124 regulates cardiomyocyte differentiation of bone marrow-derived mesenchymal stem cells via targeting STAT3 signaling. Stem Cells 30:1746–1755
56. Oliva AA, Kang Y, Sanchez-Molano J, Furones C, Atkins CM (2012) STAT3 signaling after traumatic brain injury. J Neurochem 120(5):710–720
57. Raible DJ, Frey LC, Del Angel YC, Carlsen J, Hund D, Russek SJ et al (2015) JAK/STAT pathway regulation of GABAA receptor expression after differing severities of experimental TBI. Exp Neurol 271:445–456
58. Lund IV, Hu Y, Raol YH, Benham RS, Faris R, Russek SJ et al (2008) BDNF selectively regulates GABAA receptor transcription by activation of the JAK/STAT pathway. Sci Signal 1(41):ra9
59. He M, Liu Y, Wang X, Zhang MQ, Hannon GJ, Huang ZJ (2012) Cell-type-based analysis of microRNA profiles in the mouse brain. Neuron 73(1):35–48. https://doi.org/10.1016/j.neuron.2011.11.010
60. Nesti E, Corson GM, McCleskey M, Oyer JA, Mandel G (2014) C-terminal domain small phosphatase 1 and MAP kinase reciprocally control REST stability and neuronal differentiation. Proc Natl Acad Sci USA 111(37):E3929–E3936
61. Westbrook TF, Hu G, Ang XL, Mulligan P, Pavlova NN, Liang A et al (2008) SCFβ-TRCP controls oncogenic transformation and neural differentiation through REST degradation. Nature 452(7185):370–374
62. Mandel G, Fiondella CG, Covey MV, Lu DD, LoTurco JJ, Ballas N (2011) Repressor element 1 silencing transcription factor (REST) controls radial migration and temporal neuronal specification during neocortical development. Proc Natl Acad Sci USA 108(40):16789–16794
63. Aoki H, Hara A, Era T, Kunisada T, Yamada Y (2012) Genetic ablation of REST leads to in vitro-specific derepression of neuronal genes during neurogenesis. Development (Cambridge) 139(4):667–677
64. Kok FO, Taibi A, Wanner SJ, Xie X, Moravec CE, Love CE et al (2012) Zebrafish rest regulates developmental gene expression but not neurogenesis. Development 139(20):3838–3848
65. Rodenas-Ruano A, Chávez AE, Cossio MJ, Castillo PE, Zukin RS (2012) REST-dependent epigenetic remodeling promotes the developmental switch in synaptic NMDA receptors. Nat Neurosci 15(10):1382–1390
66. Soldati C, Caramanica P, Burney MJ, Toselli C, Bithell A, Augusti-Tocco G et al (2015) RE1 silencing transcription factor/neuron-restrictive silencing factor regulates expansion of adult mouse subventricular zone-derived neural stem/progenitor cells in vitro. J Neurosci Res 93(8):1203–1214
67. Watanabe Y, Kameoka S, Gopalakrishnan V, Aldape KD, Pan ZZ, Lang FF et al (2004) Conversion of myoblasts to physiologically active neuronal phenotype. Genes Dev 18(8):889–900
68. Su X, Kameoka S, Lentz S, Majumder S (2004) Activation of REST/NRSF target genes in neural stem cells is sufficient to cause neuronal differentiation. Mol Cell Biol 24(18):8018–8025
69. Singh SK, Kagalwala MN, Parker-Thornburg J, Adams H, Majumder S (2008) REST maintains self-renewal and pluripotency of embryonic stem cells. Nature 453(7192):223–227
70. McClelland S, Brennan GP, Dubé C, Rajpara S, Iyer S, Richichi C et al (2014) The transcription factor NRSF contributes to epileptogenesis by selective repression of a subset of target genes. Elife 3:e01267
71. Chio C, Lin H, Tian Y, Chen Y, Lin M, Lin C et al (2017) Exercise attenuates neurological deficits by stimulating a critical HSP70/NF-KB/IL-6/synapsin I axis in traumatic brain injury rats. J Neuroinflamm 14(1):90
72. Malumbres M, Barbacid M (2005) Mammalian cyclin-dependent kinases. Trends Biochem Sci 30(11):630–641
73. Beukelaers P, Vandenbosch R, Caron N, Nguyen L, Belachew S, Moonen G et al (2011) Cdk6-dependent regulation of G1 length controls adult neurogenesis. Stem Cells 29(4):713–724
74. Sawicka K, Bushell M, Spriggs KA, Willis AE (2008) Polypyrimidine-tract-binding protein: a multifunctional RNA-binding protein. Biochem Soc Trans 36(4):641–647
75. Sharma S, Falick AM, Black DL (2005) Polypyrimidine tract binding protein blocks the 5′ splice site-dependent assembly of U2AF and the prespliceosomal e complex. Mol Cell 19(4):485–496
76. Markovtsov V, Nikolic JM, Goldman JA, Turck CW, Chou M, Black DL (2000) Cooperative assembly of an hnRNP complex induced by a tissue-specific homolog of polypyrimidine tract binding protein. Mol Cell Biol 20(20):7463–7479
77. Polydorides AD, Okano HJ, Yang YYL, Stefani G, Darnell RB (2000) A brain-enriched polypyrimidine tract-binding protein antagonizes the ability of Nova to regulate neuron-specific alternative splicing. Proc Natl Acad Sci USA 97(12):6350–6355
78. Licatalosi DD, Yano M, Fak JJ, Mele A, Grabinski SE, Zhang C et al (2012) Ptbp2 represses adult-specific splicing to regulate the generation of neuronal precursors in the embryonic brain. Genes Dev 26(14):1626–1642
79. Boutz PL, Stoilov P, Li Q, Lin C, Chawla G, Ostrow K et al (2007) A post-transcriptional regulatory switch in polypyrimidine tract-binding proteins reprograms alternative splicing in developing neurons. Genes Dev 21(13):1636–1652
80. Spellman R, Llorian M, Smith CWJ (2007) Crossregulation and functional redundancy between the splicing regulator PTB and its paralogs nPTB and ROD1. Mol Cell 27(3):420–434
81. Makeyev EV, Zhang J, Carrasco MA, Maniatis T (2007) The microRNA miR-124 promotes neuronal differentiation by triggering brain-specific alternative pre-mRNA splicing. Mol Cell 27(3):435–448
82. Müller S, Chakrapani BPS, Schwegler H, Hokmann H-, Kirsch M (2009) Neurogenesis in the dentate gyrus depends on ciliary neurotrophic factor and signal transducer and activator of transcription 3 signaling. Stem Cells 27(2):431–441
83. Grabenstatter HL, Del Angel YC, Carlsen J, Wempe MF, White AM, Cogswell M et al (2014) The effect of STAT3 inhibition on status epilepticus and subsequent spontaneous seizures in the pilocarpine model of acquired epilepsy. Neurobiol Dis 62:73–85
84. Kronenberg G, Gertz K, Baldinger T, Kirste I, Eckart S, Yildirim F et al (2010) Impact of actin filament stabilization on adult hippocampal and olfactory bulb neurogenesis. J Neurosci 30(9):3419–3431
85. Zhu X, Wang C, Dai P, Xie Y, Song N, Liu Y et al (2007) Myosin X regulates netrin receptors and functions in axonal path-finding. Nat Cell Biol 9(2):184–192
86. Yu H, Wang N, Ju X, Yang Y, Sun D, Lai M et al (2012) Ptdins (3,4,5) P3 recruitment of Myo10 is essential for axon development. PLoS One 7(5):e36988
87. Yu H, Sun D, Wang N, Wang M, Lan Y, Fan W et al (2015) Headless Myo10 is a regulator of microtubule stability during neuronal development. J Neurochem 135(2):261–273

88. Yu J, Chung K, Deo M, Thompson RC, Turner DL (2008) MicroRNA miR-124 regulates neurite outgrowth during neuronal differentiation. Exp Cell Res 314(14):2618–2633
89. Gu X, Li A, Liu S, Lin L, Xu S, Zhang P et al (2016) MicroRNA124 regulated neurite elongation by targeting OSBP. Mol Neurobiol 53(9):6388–6396
90. Brenes JC, Lackinger M, Höglinger GU, Schratt G, Schwarting RKW, Wöhr M (2016) Differential effects of social and physical environmental enrichment on brain plasticity, cognition, and ultrasonic communication in rats. J Comp Neurol 524(8):1586–1607
91. Stamatovic SM, Keep RF, Mostarica-Stojkovic M, Andjelkovic AV (2006) CCL2 regulates angiogenesis via activation of Ets-1 transcription factor. J Immunol 177(4):2651–2661
92. Chu HX, Arumugam TV, Gelderblom M, Magnus T, Drummond GR, Sobey CG (2014) Role of CCR2 in inflammatory conditions of the central nervous system. J Cereb Blood Flow Metab 34(9):1425–1429
93. Gyoneva S, Kim D, Katsumoto A, Kokiko-Cochran ON, Lamb BT, Ransohoff RM (2015) Ccr2 deletion dissociates cavity size and tau pathology after mild traumatic brain injury. J Neuroinflamm 12(1):228
94. Buss H, Handschick K, Jurrmann N, Pekkonen P, Beuerlein K, Müller H et al (2012) Cyclin-dependent kinase 6 phosphorylates NF-κB P65 at serine 536 and contributes to the regulation of inflammatory gene expression. PLoS One 7(12):e51847
95. Handschick K, Beuerlein K, Jurida L, Bartkuhn M, Müller H, Soelch J et al (2014) Cyclin-dependent kinase 6 is a chromatin-bound cofactor for NF-κB-dependent gene expression. Mol Cell 53(4):193–208
96. Kollmann K, Heller G, Schneckenleithner C, Warsch W, Scheicher R, Ott R et al (2013) A kinase-independent function of CDK6 links the cell cycle to tumor angiogenesis. Cancer Cell 24(2):167–181
97. Campbell IL (2005) Cytokine-mediated inflammation, tumorigenesis, and disease-associated JAK/STAT/SOCS signaling circuits in the CNS. Brain Res Rev 48(2):166–177
98. Zhong Z, Wen Z, Darnell JE Jr (1994) Stat3: a STAT family member activated by tyrosine phosphorylation in response to epidermal growth factor and interleukin-6. Science 264(5155):95–98
99. Rummel C, Hübschle T, Gerstberger R, Roth J (2004) Nuclear translocation of the transcription factor STAT3 in the guinea pig brain during systemic or localized inflammation. J Physiol 557(2):671–687
100. Lagos-Quintana M, Rauhut R, Yalcin A, Meyer J, Lendeckel W, Tuschl T (2002) Identification of tissue-specific microRNAs from mouse. Curr Biol 12(9):735–739
101. Sempere LF, Freemantle S, Pitha-Rowe I, Moss E, Dmitrovsky E, Ambros V (2004) Expression profiling of mammalian microRNAs uncovers a subset of brain-expressed microRNAs with possible roles in murine and human neuronal differentiation. Genome Biol 5(3):R13
102. Weng H, Shen C, Hirokawa G, Ji X, Takahashi R, Shimada K et al (2011) Plasma miR-124 as a biomarker for cerebral infarction. Biomed Res (Japan) 32(2):135–141
103. Nelson PT, Baldwin DA, Kloosterman WP, Kauppinen S, Plasterk RHA, Mourelatos Z (2006) RAKE and LNA-ISH reveal microRNA expression and localization in archival human brain. RNA 12(2):187–191
104. Brennan GP, Dey D, Chen Y, Patterson KP, Magnetta EJ, Hall AM et al (2016) Dual and opposing roles of microRNA-124 in epilepsy are mediated through inflammatory and NRSF-dependent gene networks. Cell Rep 14(10):2402–2412
105. Suzhi Z, Liang T, Yuexia P, Lucy L, Xiaoting H, Yuan Z et al (2015) Gap junctions enhance the antiproliferative effect of microRNA-124-3p in glioblastoma cells. J Cell Physiol 230(10):2476–2488
106. Lunavat TR, Cheng L, Kim D-, Bhadury J, Jang SC, Lässer C et al (2015) Small RNA deep sequencing discriminates subsets of extracellular vesicles released by melanoma cells—evidence of unique microRNA cargos. RNA Biol 12(8):810–823
107. Gorter JA, Iyer A, White I, Colzi A, van Vliet EA, Sisodiya S et al (2014) Hippocampal subregion-specific microRNA expression during epileptogenesis in experimental temporal lobe epilepsy. Neurobiol Dis 62:508–520
108. Hu K, Zhang C, Long L, Long X, Feng L, Li Y et al (2011) Expression profile of microRNAs in rat hippocampus following lithium–pilocarpine-induced status epilepticus. Neurosci Lett 488(3):252–257
109. Kochanek PM, Dixon CE, Shellington DK, Shin SS, Bayir H, Jackson EK et al (2013) Screening of biochemical and molecular mechanisms of secondary injury and repair in the brain after experimental blast-induced traumatic brain injury in rats. J Neurotrauma 30(11):920–937
110. Attilio PJ, Flora M, Kamnaksh A, Bradshaw DJ, Agoston D, Mueller GP (2017) The effects of blast exposure on protein deimination in the brain. Oxid Med Cell Longev. https://doi.org/10.1155/2017/8398072
111. Sun HT, Cheng SX, Tu Y, Li XH, Zhang S (2013) FoxQ1 promotes glioma cells proliferation and migration by regulating NRXN3 expression. PLoS One 8(1):e55693
112. Ostrowski M, Carmo NB, Krumeich S, Fanget I, Raposo G, Savina A et al (2010) Rab27a and Rab27b control different steps of the exosome secretion pathway. Nat Cell Biol 12(1):19–30
113. Yuan L, Sacharidou A, Stratman AN, Le Bras A, Zwiers PJ, Spokes K et al (2011) RhoJ is an endothelial cell-restricted Rho GTPase that mediates vascular morphogenesis and is regulated by the transcription factor ERG. Blood 118(4):1145–1153
114. Zhang L, Wang T, Valle D (2015) Reduced PLP2 expression increases ER-stress-induced neuronal apoptosis and risk for adverse neurological outcomes after hypoxia ischemia injury. Hum Mol Genet 24(25):7221–7226
115. Wang G, Nikolovska-Coleska Z, Yang C, Wang R, Tang G, Guo J et al (2006) Structure-based design of potent small-molecule inhibitors of anti-apoptotic Bcl-2 proteins. J Med Chem 49(21):6139–6142
116. Soderholm JF, Bird SL, Kalab P, Sampathkumar Y, Hasegawa K, Uehara-Bingen M et al (2011) Importazole, a small molecule inhibitor of the transport receptor importin-β. ACS Chem Biol 6(7):700–708
117. Görlich D, Prehn S, Laskey RA, Hartmann E (1994) Isolation of a protein that is essential for the first step of nuclear protein import. Cell 79(5):767–778
118. Forbes DJ, Travesa A, Nord MS, Bernis C (2015) Nuclear transport factors: global regulation of mitosis. Curr Opin Cell Biol 35:78–90
119. Jost PJ, Ruland J (2007) Aberrant NF-κB signaling in lymphoma: mechanisms, consequences, and therapeutic implications. Blood 109(7):2700–2707
120. Mackowiak B, Li L, Welch MA, Li D, Jones JW, Heyward S et al (2017) Molecular basis of metabolism-mediated conversion of PK11195 from an antagonist to an agonist of the constitutive androstane receptor. Mol Pharmacol 92(1):75–87
121. Kletsas D, Li W, Han Z, Papadopoulos V (2004) Peripheral-type benzodiazepine receptor (PBR) and PBR drug ligands in fibroblast and fibrosarcoma cell proliferation: role of ERK, c-Jun and ligand-activated PBR-independent pathways. Biochem Pharmacol 67(10):1927–1932
122. Carmel I, Fares FA, Leschiner S, Scherübl H, Weisinger G, Gavish M (1999) Peripheral-type benzodiazepine receptors in the

regulation of proliferation of MCF-7 human breast carcinoma cell line. Biochem Pharmacol 58(2):273–278
123. Folkersma H, Boellaard R, Vandertop WP, Kloet RW, Lubberink M, Lammertsma AA et al (2009) Reference tissue models and blood–brain barrier disruption: lessons from (R)-[11C]PK11195 in traumatic brain injury. J Nucl Med 50(12):1975–1979
124. Mitsiades CS, Mitsiades NS, McMullan CJ, Poulaki V, Shringarpure R, Hideshima T et al (2004) Transcriptional signature of histone deacetylase inhibition in multiple myeloma: biological and clinical implications. Proc Natl Acad Sci USA 101(2):540–545
125. Siegel D, Hussein M, Belani C, Robert F, Galanis E, Richon VM et al (2009) Vorinostat in solid and hematologic malignancies. J Hematol Oncol 2:31
126. Vrana JA, Decker RH, Johnson CR, Wang Z, Jarvis WD, Richon VM et al (1999) Induction of apoptosis in U937 human leukemia cells by suberoylanilide hydroxamic acid (SAHA) proceeds through pathways that are regulated by Bcl-2/Bcl-x(L), c-Jun, and p21(CIP1), but independent of p53. Oncogene 18(50):7016–7025
127. He L, Tolentino T, Grayson P, Zhong S, Warrell RP Jr, Rifkind RA et al (2001) Histone deacetylase inhibitors induce remission in transgenic models of therapy-resistant acute promyelocytic leukemia. J Clin Investig 108(9):1321–1330
128. Peiffer L, Poll-Wolbeck SJ, Flamme H, Gehrke I, Hallek M, Kreuzer K (2014) Trichostatin A effectively induces apoptosis in chronic lymphocytic leukemia cells via inhibition of Wnt signaling and histone deacetylation. J Cancer Res Clin Oncol 140(8):1283–1293
129. Nguyen M, Marcellus RC, Roulston A, Watson M, Serfass L, Murthy Madiraju SR et al (2007) Small molecule obatoclax (GX15-070) antagonizes MCL-1 and overcomes MCL-1-mediated resistance to apoptosis. Proc Natl Acad Sci USA 104(49):19512–19517
130. Liu Q, Chang JW, Wang J, Kang SA, Thoreen CC, Markhard A et al (2010) Discovery of 1-(4-(4-Propionylpiperazin-1-yl)-3-(trifluoromethyl)phenyl)-9-(quinolin-3-yl)benzo[h][1,6]naphthyridin-2(1 H)-one as a highly potent, selective mammalian target of rapamycin (mTOR) inhibitor for the treatment of cancer. J Med Chem 53(19):7146–7155
131. Kumar S, Guru SK, Venkateswarlu V, Malik F, Vishwakarma RA, Sawant SD et al (2015) A novel quinoline based second-generation mTOR inhibitor that induces apoptosis and disrupts PI3K-Akt-mTOR signaling in human leukemia HL-60 cells. Anti Cancer Agents Med Chem 15(10):1297–1304
132. Yu H, Qiu Y, Pang X, Li J, Wu S, Yin S et al (2017) Lycorine promotes autophagy and apoptosis via TCRP1/Akt/mTOR axis inactivation in human hepatocellular carcinoma. Mol Cancer Ther 16(12):2711–2723
133. Guo D, Zeng L, Brody DL, Wong M (2013) Rapamycin attenuates the development of posttraumatic epilepsy in a mouse model of traumatic brain injury. PLoS One 8(5):e64078
134. Butler CR, Boychuk JA, Smith BN (2015) Effects of rapamycin treatment on neurogenesis and synaptic reorganization in the dentate gyrus after controlled cortical impact injury in mice. Front Syst Neurosci 9:163
135. Kotulska K, Chmielewski D, Borkowska J, Jurkiewicz E, Kuczyński D, Kmieć T et al (2013) Long-term effect of everolimus on epilepsy and growth in children under 3 years of age treated for subependymal giant cell astrocytoma associated with tuberous sclerosis complex. Eur J Paediatr Neurol 17(5):479–485
136. Franz DN, Belousova E, Sparagana S, Bebin EM, Frost M, Kuperman R et al (2014) Everolimus for subependymal giant cell astrocytoma in patients with tuberous sclerosis complex: 2-year open-label extension of the randomised EXIST-1 study. Lancet Oncol 15(13):1513–1520
137. Cardamone M, Flanagan D, Mowat D, Kennedy SE, Chopra M, Lawson JA (2014) Mammalian target of rapamycin inhibitors for intractable epilepsy and subependymal giant cell astrocytomas in tuberous sclerosis complex. J Pediatr 164(5):1195–1200
138. Racke FK, Baird M, Barth RF, Huo T, Yang W, Gupta N, Weldon M, Rutledge H (2012) Unique in vitro and in vivo thrombopoietic activities of ingenol 3,20 dibenzoate, A Ca^{2+}-independent protein kinase C isoform agonist. PLoS One 7(12):e51059
139. Jiang H, Cheng D, Liu W, Peng J, Feng J (2010) Protein kinase C inhibits autophagy and phosphorylates LC3. Biochem Biophys Res Commun 395(4):471–476